ENGINEERING TECHNICAL REPORT

IQ Modulation

Fundamentals, analysis of non-idealities and compensation techniques

Franco A. Alcaraz

Version 2.0
June 5, 2015

It includes explicit conventions, general models, calibration procedures and numerical examples. The figures are computed from their equations; the results presented are analytical and simulated, and no experimental hardware validation is claimed for them.

Abstract

Quadrature modulation makes it possible to represent a real bandpass signal by means of a baseband complex envelope. Its implementation with two DACs, filters and mixers introduces errors that can produce carrier leakage, image components and frequency-dependent distortion.

This report establishes a uniform modulation and Fourier convention, derives the generation of tones and linear chirps and analyzes the zero-order-hold response. It then studies DC offsets, gain imbalance, the quadrature error of the local oscillator, coupling between branches and differential delay. Capacitive coupling is obtained from an equivalent circuit and compared with its nodal solution, avoiding the assignment of universal responses to parasitic mechanisms whose impedances are unknown.

A distinction is made between amplitude, power, image level and image rejection ratio. A model with a conjugate term gathers the linear errors and allows a predistortion and a calibration strategy to be formulated. The report closes with application limits and conclusions.

Keywords: IQ modulation, complex envelope, image rejection, carrier leakage, calibration, predistortion, linear chirp.

Contents

Abstract **i**

1 Objectives, scope and conventions **1**

1.1 Purpose of the report . . . 1
1.2 Scope and assumptions . . . 1
1.3 Modulation and transform convention . . . 1
1.4 Symbols and quantities . . . 2
1.5 Graphical conventions . . . 2

2 Fundamentals of IQ modulation **3**

2.1 Complex envelope and vector representation . . . 3
2.2 Frequency conversion and real spectrum . . . 3
2.3 Baseband recovery . . . 5
2.4 Modulation of a pure tone . . . 5
2.5 Bandwidth and sampling . . . 7
2.6 Finite-duration linear chirp . . . 7

3 Implementation and DAC response **10**

3.1 Generation chain . . . 10
3.2 Zero-order hold and sinc . . . 10
3.3 Compensation within the band of interest . . . 11

4 DC offsets and carrier leakage **13**

4.1 Offset model . . . 13
4.2 Digital and analog compensation . . . 13
4.3 Searching for the minimum . . . 16

5 Gain imbalance **17**

5.1 General model with a conjugate component . . . 17
5.2 Tone and elliptical trajectory . . . 17
5.3 Metrics and examples . . . 19
5.4 Compensation and resolution limit . . . 19

6 Local oscillator quadrature error **21**
6.1 Mixer model . . . 21
6.2 Tone, image and common phase . . . 22
6.3 Simultaneous gain and phase errors . . . 23

7 Coupling between baseband branches **25**
7.1 LTI model and the need for an equivalent circuit . . . 25
7.2 Asymmetric cross-coupling . . . 26
7.3 Symmetric capacitive circuit . . . 26
7.4 Magnitude, phase and modulated signal . . . 30

8 Differential delay and combined error **34**
8.1 Delays in the baseband branches . . . 34
8.2 Image level and narrowband approximation . . . 36
8.3 Simultaneous LO quadrature error and delay . . . 36
8.4 Phase delay and group delay . . . 37

9 Unified model and predistortion **40**
9.1 Model with a conjugate term . . . 40
9.2 Inversion of the constant model . . . 40
9.3 Frequency-dependent extension . . . 40
9.4 Practical order of the corrections . . . 41

10 Calibration and verification procedure **42**
10.1 Measurement preparation . . . 42
10.2 Proposed sequence . . . 42
10.3 FFT, coherence, and normalization . . . 43
10.4 Acceptance criteria and limits . . . 43

11 Conclusions **44**

Bibliography **45**

List of Figures

2.1 Vector representation: (a) coordinates $I(t)$ and $Q(t)$ of the envelope $A_m e^{j\omega_m t}$; (b) in the frame rotating at f_0, a component at $f_0 + f_m$ rotates at $+\omega_m$ and one at $f_0 - f_m$ rotates at $-\omega_m$. 4

2.2 Spectrum of a generic envelope of width W (left) and of the real RF signal (right), in magnitude and phase. The replica at $-f_0$ is $\frac{1}{2}B^*(-f - f_0)$: it is mirrored and its phase changes sign. 4

2.3 Modulation process for an envelope with real $B(f)$: decomposition into $I_f(f)$ (even part) and $jQ_f(f)$ (odd part), mixing with the carriers and summation of both branches. 5

2.4 Line spectrum of an ideal tone. In baseband there is a single line at f_m; the real RF signal contains $\frac{1}{2}A_m$ at $f_0 + f_m$ and its conjugate replica at $-f_0 - f_m$. 6

2.5 Ideal tone: $f_0 = 1\,\text{MHz}$, $f_m = 125\,\text{kHz}$, $f_s = 4\,\text{MHz}$ and $A_m = 1$. The two-sided spectrum shows the replicas necessarily present in a real RF signal. 6

2.6 LFM chirp with $T = 250\,\mu\text{s}$ and an excursion from $f_a = -25$ to $f_b = +25\,\text{kHz}$. Its spectrum shows ripple and energy outside the sweep interval due to its finite duration and window. 8

2.7 Schematic translation of a chirp of width $W = f_b - f_a$. Color indicates the instant at which each frequency is visited; the constant height is only the rectangular-spectrum approximation. 8

2.8 RF simulation of a centered 50 kHz chirp of $1024\,\mu\text{s}$ duration, with $f_0 = 1\,\text{MHz}$. The amplitude of each spectral bin depends on the duration and is referenced to $A_m/2$; it is not to be interpreted as the level of a tone. 9

3.1 IQ modulator with DACs: conversion with a common clock, amplification, reconstruction filtering (LPF), mixing with the quadrature LO, summation and RF filtering (BPF). The signs correspond to equation (1.1); an implementation may incorporate the sign into the LO. 10

3.2 Output of a DAC with zero-order hold at $f_s = 60\,\text{MHz}$ (one-sided view of a real signal) for tones at 8, 16 and 25 MHz: (a) without compensation; (b) with amplitude pre-compensation limited to the band of interest and normalized to the band-edge level. 11

3.3 Magnitude of the zero-order hold and pre-compensation limited to $\pm 25\,\text{MHz}$ for $f_s = 60\,\text{MHz}$. 12

4.1 Phasor representation of an offset $O = 0.3A_m$ with $\theta_O = 36.9°$, exaggerated for readability. The vector O is static in the LO frame and shifts the center of the trajectory. 14

4.2 Spectra with a DC offset $O = 0.3A_m$: (a) generic envelope; (b) tone. The leakage appears exactly at f_0 and at its replica $-f_0$. 14

4.3 Offsets $O_I = 0.04$ and $O_Q = 0.03$ for $A_m = 1$. The RF component at f_0 lies at $-26.02\,\text{dBc}$. 15

4.4 Offset correction: digital adjustment added to the sequences before the DACs (dashed line) or analog adjustment through auxiliary DACs after the signal DACs. 15

5.1 Gain imbalance with $G_I = 1.2$ and $G_Q = 0.7$: (a) elliptical trajectory and projections $G_I I(t)$ and $G_Q Q(t)$; (b) decomposition into a desired component and an image rotating in opposite directions. 18

5.2 Case $G_I = 1.05$, $G_Q = 0.95$: unit desired amplitude and an image of amplitude 0.05, equivalent to $-26.02\,\text{dBc}$. 18

5.3 Line spectrum with $G_I = 0.95$ and $G_Q = 0.70$: $|D| = 0.825A_m$ and image $|E| = 0.125A_m$, i.e., $-16.39\,\text{dBc}$. The dashed line indicates the nominal level. 19

5.4 Image level and desired-signal gain as $G_I - G_Q$ varies, with $G_Q = 1$. The image reference is the actual desired signal. 20

6.1 Quadrature error in the local oscillator: the splitter outputs exhibit deviations ϕ_I and ϕ_Q from their nominal phases. 21

6.2 Quadrature error with $\phi_I = 27°$ and $\phi_Q = 9°$: (a) non-orthogonal effective axes; (b) desired and image components. The major axis of the ellipse does not coincide with the I and Q axes. 22

6.3 Line spectrum for the case of figure 6.2: the desired line has phase $\bar{\phi} = 18°$ and the image has phase $\bar{\phi} + 90° = 108°$, with magnitudes $\cos(\Delta\phi/2)$ and $\sin(\Delta\phi/2)$. . . . 22

6.4 Errors $\phi_I = 27°$ and $\phi_Q = 9°$: $\Delta\phi = 18°$, a common rotation of 18° and an image at approximately $-16.01\,\text{dBc}$. 23

6.5 Image rejection for quadrature errors between 0.01° and 5°. At zero, the ideal model has infinite rejection; a physical system is limited by other errors. 24

7.1 Coupling between baseband branches represented by the matrix $H(f)$ of equation (7.1). The cross-coupling terms are $K_{I\to Q} = H_{QI}$ and $K_{Q\to I} = H_{IQ}$. 25

7.2 Trajectories for symmetric cross-coupling $B_{\text{sal}} = B + jKB^*(-f)$ with $|K| = 0.25$. Top row: constant, derivative and integrating terms. Bottom row: $K = 0.15 + 0.1j\omega + 0.1/(j\omega)$ at two normalized frequencies, $\omega_{m1} = 0.5$ and $\omega_{m2} = 2$. The dotted line indicates the major axis. 27

7.3 Unequal direct cross-coupling terms: $K_{I\to Q} = 0.1$ and $K_{Q\to I} = 0.2$. The direct coefficient is $1 - 0.05j$ and the image coefficient is $0.15j$. 28

7.4 Swapping of the I and Q signals: the tone $b(t) = A_m e^{j\omega_m t}$ becomes $jb^*(t)$, which starts at 90° (green dot) and rotates in the negative direction. 28

7.5 Lumped circuit of capacitive coupling between symmetric branches. When an ideal voltage source is deactivated, its series resistance remains connected to ground. . . 29

7.6 Superposition in the circuit of figure 7.5: (a) the I branch couples into the Q branch; (b) the Q branch couples into the I branch. The deactivated source leaves its series resistance connected to ground. 29

7.7 Amplitudes referred to the nominal signal, and phases of the transfer functions of the symmetric circuit. The phase of the cross transfer function is not directly the phase of the RF image. 30

7.8 Desired (blue) and image (red) components of the symmetric capacitive circuit for $x = 0.05$, 0.5 and 5. The dotted line indicates the 45° direction. 31

7.9 Envelope trajectories for different values of x. Strong coupling collapses the ellipse into a straight line at 45°; the desired component and the image have equal magnitude. 32

7.10 Time-domain and spectral example with $R_S = R_L = 50\,\Omega$, $C_M = 5\,\mathrm{nF}$ and $f_m = 125\,\mathrm{kHz}$. The sources are normalized to obtain $A_m = 1$ without coupling. . . 32

7.11 Spectrum of two tones of equal nominal amplitude in the capacitive circuit, with $x_1 = \omega_{m1}\tau_C = 0.1$ and $x_2 = \omega_{m2}\tau_C = 0.5$. The levels are computed with equation (7.8). 33

8.1 Time delays τ_I and τ_Q in the baseband branches, before the mixers. 34

8.2 Delays $\tau_I = 0.7\,\mu\mathrm{s}$ and $\tau_Q = 0.2\,\mu\mathrm{s}$ at $f_m = 125\,\mathrm{kHz}$. The image grows with the product of the baseband frequency and the differential delay. 35

8.3 Trajectories for $\tau_I = 0.7\,\mu\mathrm{s}$ and $\tau_Q = 0.2\,\mu\mathrm{s}$ at three baseband frequencies. The dotted square marks the amplitudes of I and Q, which the delay does not modify. . 35

8.4 Desired signal and image, referred to the nominal amplitude, as a function of the product $f_m\Delta\tau$: (a) linear scale, with periodic zeros and maxima; (b) logarithmic scale and narrowband approximation. The dot marks the example of 40 dB up to 25 MHz. 36

8.5 With $\Delta\tau = 0.5\,\mu\mathrm{s}$ and $\Delta\phi = -9°$, the minimum shifts to 50 kHz. The plot distinguishes the nominal reference from the actual desired signal. 37

8.6 Three tones with $\Delta\tau = 0.5\,\mu\mathrm{s}$: (a) baseband; (b) RF with $\Delta\phi = -9°$, whose image null coincides with $f_{m2} = 50\,\mathrm{kHz}$ (×); (c) RF with $\Delta\phi = 0$. Levels referred to the nominal amplitude. 38

8.7 Example filters: Butterworth filter of order 4 and a four-stage all-pass cascade, with explicit coefficients. 39

8.8 Alternating train of tones at 125 and 250 kHz, filtered with an example all-pass. The frequency-dependent delay modifies the temporal alignment of the pulses. . . . 39

List of Tables

1.1 Main symbols. 2

5.1 Gain imbalance examples. 19

7.1 Capacitive circuit: values computed with equation (7.8). D/A_m and E/A_m denote relative magnitudes. 30

Chapter 1

Objectives, scope and conventions

1.1 Purpose of the report

The aim is to link the errors observable at the output of an IQ modulator with models that make it possible to understand, estimate and compensate them. The approach is didactic: start from the ideal signal, introduce a non-ideality and explain its effect through equations, spectra and trajectories in the complex plane.

The intended reader is an engineer or student familiar with signals, Fourier analysis and linear circuits. The report can help prepare a calibration or a simulation, but it does not specify a complete hardware design nor the acceptance of any particular product.

1.2 Scope and assumptions

Unless otherwise stated, the mixers are assumed to be ideal and linear, the sources coherent, the gains constant and the local oscillator of fixed frequency. Frequency-dependent responses are modeled as linear time-invariant (LTI) systems. Offsets are constant during each measurement. Temperature, LO frequency and drive level may change the parameters between measurements.

Compression, intermodulation products, phase noise, clock jitter, quantization and DAC switching transients are left out of the quantitative treatment. These mechanisms can limit a calibration even after the linear model has been compensated. The numerical tables and figures illustrate models; they do not correspond to measurements of a physical modulator.

1.3 Modulation and transform convention

A complex envelope $b(t) = I(t) + jQ(t)$ is used, with I and Q real, and the following real output:

$$s(t) = \mathrm{Re}\{b(t)e^{j2\pi f_0 t}\} = I(t)\cos(2\pi f_0 t) - Q(t)\sin(2\pi f_0 t). \tag{1.1}$$

Implementations that add $Q\sin$ instead of subtracting it use a different convention: to carry their formulas over, the sign of Q must be changed. The two conventions must not be mixed within a derivation.

The Fourier transform is defined as

$$X(f) = \int_{-\infty}^{\infty} x(t)e^{-j2\pi ft}\,dt, \qquad x(t) = \int_{-\infty}^{\infty} X(f)e^{j2\pi ft}\,df. \tag{1.2}$$

When $\omega = 2\pi f$ is used, derivatives transform into factors $j\omega$ and delays into $e^{-j\omega\tau}$. All angles in equations are in radians; plots in degrees say so explicitly.

1.4 Symbols and quantities

Table 1.1: Main symbols.

Symbol	Meaning
$b(t)$, $B(f)$	Complex envelope and its transform
$s(t)$, $S(f)$	Real RF signal and its transform
f_0, f_m, f_s	LO, baseband tone and sampling frequencies
A_m	Nominal envelope amplitude of a tone
G_I, G_Q	Linear gains of the branches
O_I, O_Q	Input-referred DC offsets
ϕ_I, ϕ_Q	Phase errors added to the LO components
τ_I, τ_Q	Time delays of the baseband branches
D, E	Complex coefficients of the desired signal and image
H_{xy}	Transfer from branch y to branch x

For two sinusoids across the same load, the power ratio is the square of the amplitude ratio. The following are defined:

$$L_{\text{img}} = 10\log_{10}\frac{P_{\text{img}}}{P_{\text{des}}} = 20\log_{10}\left|\frac{E}{D}\right| \quad [\text{dBc}], \tag{1.3}$$

$$\text{IRR} = 10\log_{10}\frac{P_{\text{des}}}{P_{\text{img}}} = -L_{\text{img}} \quad [\text{dB}]. \tag{1.4}$$

An image level of $-40\,\text{dBc}$ is equivalent to an image rejection of $40\,\text{dB}$. This convention is kept throughout the report. The reference must be stated if the comparison is made against a nominal amplitude rather than against the actual desired signal.

1.5 Graphical conventions

The IQ planes are drawn in the frame rotating at f_0. Blue vectors represent the desired component, red vectors the image and gray vectors the offset or LO leakage. The vectors are chained, so their sum traces the envelope trajectory. A short arc next to each vector indicates its direction of rotation: $+\omega_m$ for the desired component and $-\omega_m$ for the image; the offset is static in that frame. When a vector is small compared with the scale of the plane, an inset magnifies the marked region. Its ΔRe and ΔIm axes are coordinates relative to the origin of that vector: the magnification preserves geometry and amplitudes and only adapts the arrow thickness.

Line spectra use the same color code. Heights are linear magnitudes unless the axis indicates dB, and the $-f_0$ replica of the real signal is drawn with magnitude $\frac{1}{2}|B^*(-f - f_0)|$. When a parameter is exaggerated for readability, the caption says so.

Chapter 2

Fundamentals of IQ modulation

2.1 Complex envelope and vector representation

The I and Q channels are coordinates on orthogonal axes. This orthogonality does not require their waveforms to be offset in time by 90°: they can be two arbitrary real functions. The sine/cosine relationship appears in the particular case of a complex tone. This distinction allows the analysis to be extended to digital signals, chirps and variable-amplitude envelopes [1].

The amplitude and phase of the envelope are

$$|b(t)| = \sqrt{I^2(t) + Q^2(t)}, \qquad \arg b(t) = \operatorname{atan2}(Q(t), I(t)). \tag{2.1}$$

The ratio Q/I alone does not identify the quadrant, and its arctangent fails when $I = 0$. At the origin the phase is undefined. Phase unwrapping removes 2π jumps, but it does not recover a meaningful phase for samples with zero magnitude or dominated by noise.

In a frame rotating at f_0, the vector $b(t)$ rotates only at the offset frequency relative to the LO. An image at frequency $f_0 - f_m$ rotates at $-f_m$ in that frame, even though its RF frequency is still positive. Confusing these frames leads to misinterpreting the directions of rotation. Figure 2.1 shows both ideas for a tone: the decomposition of the vector into its coordinates $I(t)$ and $Q(t)$, and the direction of rotation of components located above and below the LO.

2.2 Frequency conversion and real spectrum

Taking the real part of the complex signal is equivalent to

$$s(t) = \frac{1}{2} b(t) e^{j2\pi f_0 t} + \frac{1}{2} b^*(t) e^{-j2\pi f_0 t}. \tag{2.2}$$

The conjugation property and the frequency shift give

$$S(f) = \frac{1}{2} B(f - f_0) + \frac{1}{2} B^*(-f - f_0). \tag{2.3}$$

The term around $+f_0$ is a translation of the complex spectrum; the one at $-f_0$ is its conjugate, mirrored replica. The relation $S(-f) = S^*(f)$ holds, as befits a real signal. The 1/2 factors are needed if spectral amplitudes are represented on an absolute scale. Figure 2.2 illustrates this for a generic envelope of width W: the replica at $+f_0$ keeps the shape of $B(f)$, while the one at $-f_0$ appears mirrored in frequency and with its phase sign reversed.

Nor are the transforms of the channels, in general, the pointwise real and imaginary parts of $B(f)$:

$$I_f(f) = \frac{B(f) + B^*(-f)}{2}, \qquad Q_f(f) = \frac{B(f) - B^*(-f)}{2j}. \tag{2.4}$$

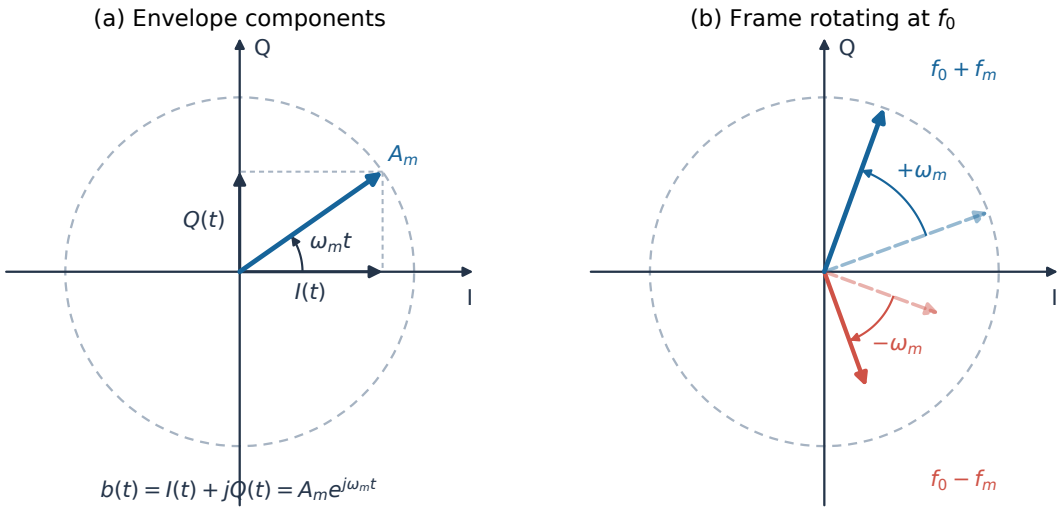

Figure 2.1: Vector representation: (a) coordinates $I(t)$ and $Q(t)$ of the envelope $A_m e^{j\omega_m t}$; (b) in the frame rotating at f_0, a component at $f_0 + f_m$ rotates at $+\omega_m$ and one at $f_0 - f_m$ rotates at $-\omega_m$.

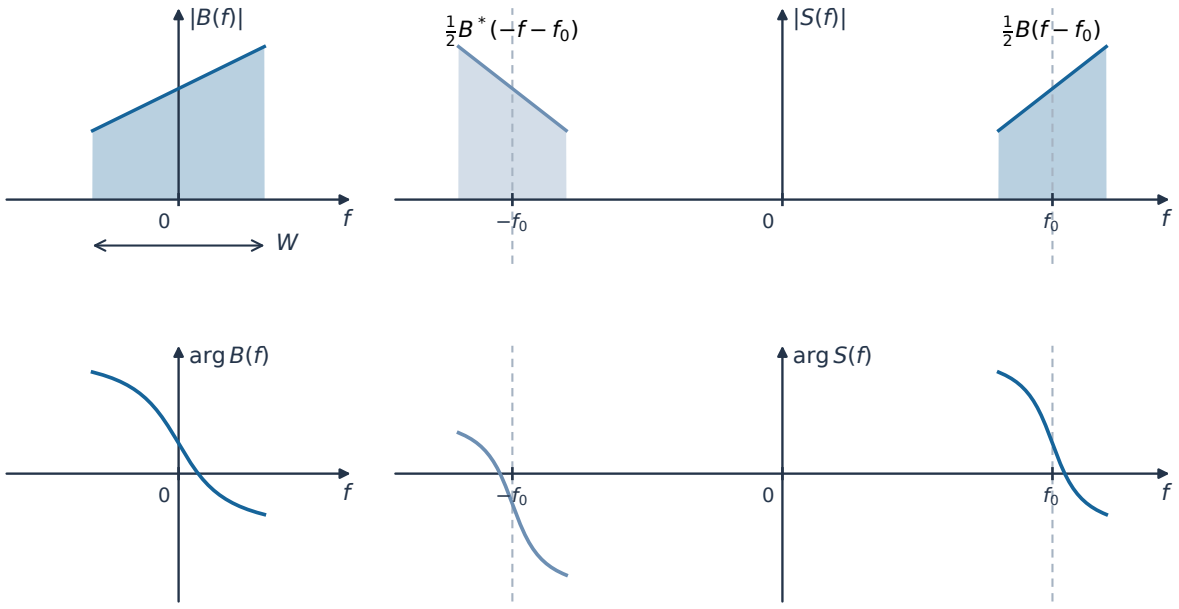

Figure 2.2: Spectrum of a generic envelope of width W (left) and of the real RF signal (right), in magnitude and phase. The replica at $-f_0$ is $\frac{1}{2}B^*(-f - f_0)$: it is mirrored and its phase changes sign.

Each has Hermitian symmetry, because I and Q are real signals.

The complete process is shown in figure 2.3. To draw the spectra as signed real quantities, an envelope with real $B(f)$ is chosen; then $I_f(f)$ is the even part of $B(f)$ and $jQ_f(f)$ its odd part. The Q branch is written as $[jQ(t)]\,[j\sin\omega_0 t] = -Q(t)\sin\omega_0 t$, and the carrier $j\sin\omega_0 t$ has lines of $+\frac{1}{2}$ at f_0 and $-\frac{1}{2}$ at $-f_0$. The odd part adds around $+f_0$ and enters with the opposite sign around $-f_0$; the sum of both branches reproduces equation (2.3).

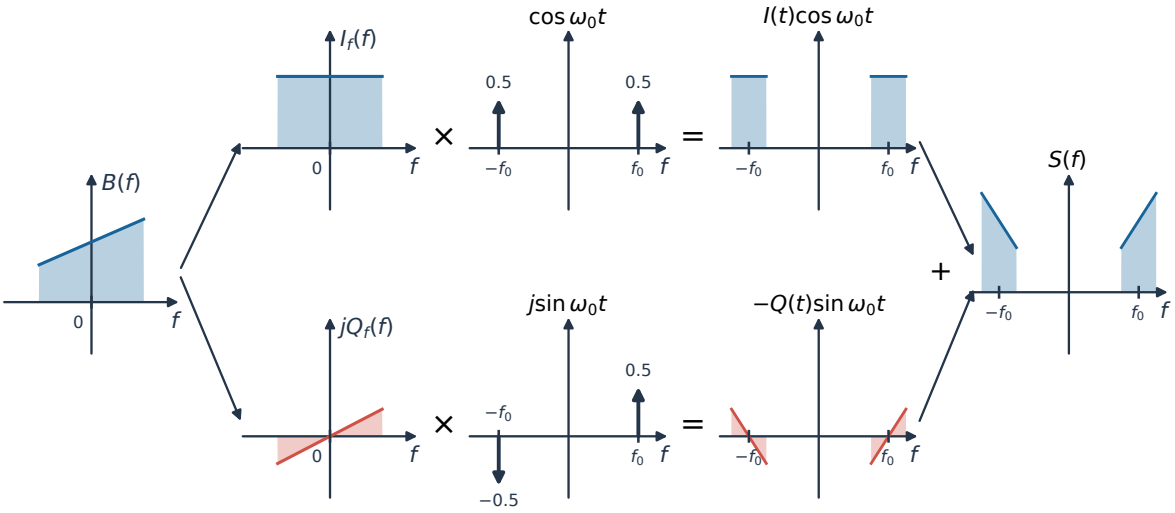

Figure 2.3: Modulation process for an envelope with real $B(f)$: decomposition into $I_f(f)$ (even part) and $jQ_f(f)$ (odd part), mixing with the carriers and summation of both branches.

2.3 Baseband recovery

Multiplying the real signal by a negative-frequency exponential,

$$s(t)e^{-j2\pi f_0 t} = \frac{1}{2}b(t) + \frac{1}{2}b^*(t)e^{-j4\pi f_0 t}. \tag{2.5}$$

If the lowpass filter separates both components, the recovery is

$$b(t) = 2\,\mathrm{LPF}\{s(t)e^{-j2\pi f_0 t}\}. \tag{2.6}$$

In frequency, with $H_{\mathrm{LPF}}(f)$ equal to unity in the band of interest,

$$B(f) = 2H_{\mathrm{LPF}}(f)S(f + f_0). \tag{2.7}$$

The factor 2 normalizes the envelope according to equation (1.1); it does not represent power that can be recovered for free by filtering. A different gain is possible, but it must be stated and kept throughout the chain.

2.4 Modulation of a pure tone

To obtain $s(t) = A_m \cos[2\pi(f_0 + f_m)t + \theta_0]$, choose

$$b(t) = A_m e^{j(2\pi f_m t + \theta_0)}, \tag{2.8}$$

$$I(t) = A_m \cos(2\pi f_m t + \theta_0), \qquad Q(t) = A_m \sin(2\pi f_m t + \theta_0). \tag{2.9}$$

Substituting into equation (1.1), the components at $f_0 - f_m$ cancel and those at $f_0 + f_m$ add. A negative f_m generates the tone below the LO. A constant-magnitude tone traces a circle in the envelope plane. The corresponding line spectrum is sketched in figure 2.4; figure 2.5 shows the simulation with specific parameters.

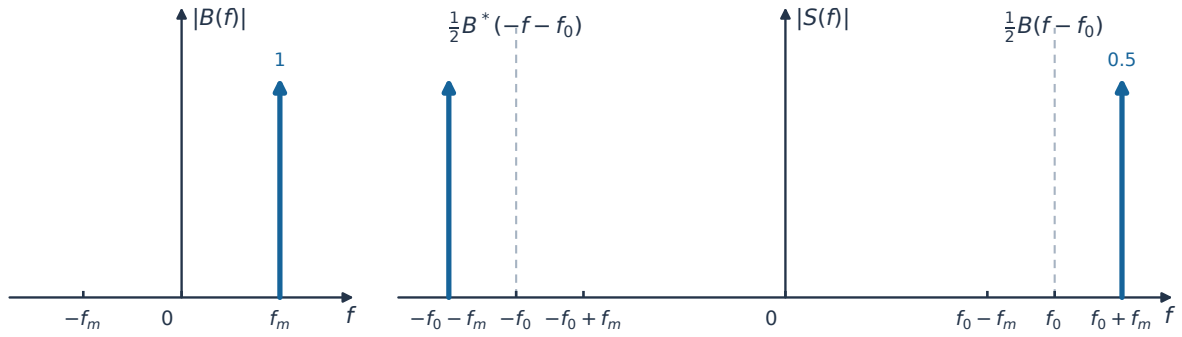

Figure 2.4: Line spectrum of an ideal tone. In baseband there is a single line at f_m; the real RF signal contains $\frac{1}{2}A_m$ at $f_0 + f_m$ and its conjugate replica at $-f_0 - f_m$.

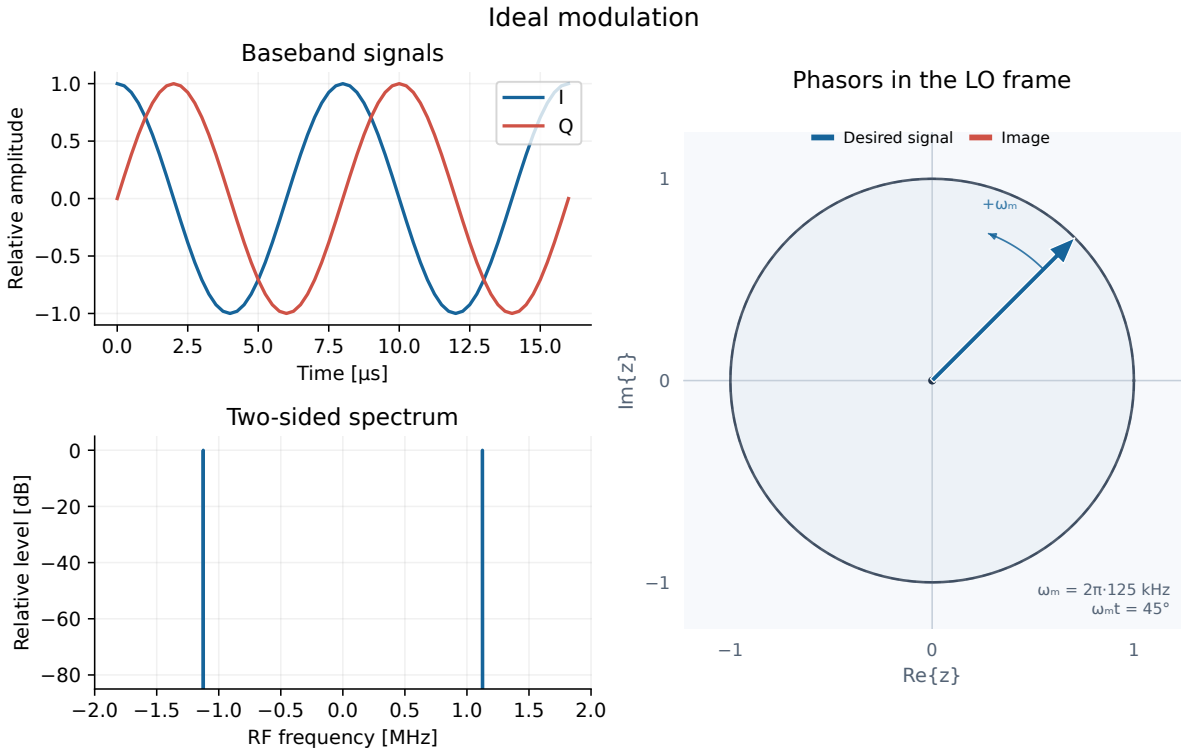

Figure 2.5: Ideal tone: $f_0 = 1\,\text{MHz}$, $f_m = 125\,\text{kHz}$, $f_s = 4\,\text{MHz}$ and $A_m = 1$. The two-sided spectrum shows the replicas necessarily present in a real RF signal.

For N samples, $n = 0, \ldots, N-1$, the discrete-time expression is

$$b[n] = A_m e^{j(2\pi f_m n/f_s + \theta_0)}. \tag{2.10}$$

A table that repeats without a phase discontinuity requires $f_m N/f_s$ to be an integer. Otherwise, a jump appears when the table is repeated and, consequently, so do additional spectral components.

2.5 Bandwidth and sampling

If $B(f)$ occupies $[-W/2, W/2]$, each real channel must represent frequencies up to $W/2$, and $f_s > W$ is required per channel to leave margin for the reconstruction filter. There is no universal factor-of-two reduction with respect to every RF architecture: the outcome depends on direct sampling, on possible bandpass sampling and on the spectral location of the signal.

The complex representation allows two real sequences at a baseband rate to be used. It does not remove the two values per complex sample. To simulate the RF directly as a real signal, without aliasing or bandpass sampling, $f_s > 2(f_0 + W/2)$ is additionally required. The simulations in this report meet that condition whenever they compute the RF.

2.6 Finite-duration linear chirp

A chirp is a signal whose instantaneous frequency varies with time. The linear case (LFM) is studied here. For $u = t - t_a$ and $0 \le u < T$,

$$k = \frac{f_b - f_a}{T}, \qquad f(u) = f_a + ku, \tag{2.11}$$

$$\theta(u) = \theta_0 + 2\pi \left(f_a u + \frac{k}{2} u^2 \right), \tag{2.12}$$

$$b(t) = A_m w(u) e^{j\theta(u)}. \tag{2.13}$$

$w(u)$ is a finite-duration window. With $w = 1$ within the interval and zero outside, the chirp has abrupt edges. To center the sweep, $f_a = -W/2$, $f_b = W/2$ are used, where $W = |f_b - f_a|$. For a downward sweep the sign of k is kept; a negative excursion must not be replaced by a positive bandwidth without adjusting the chirp law.

The discrete-time version with $T = N/f_s$ is

$$\theta[n] = \theta_0 + 2\pi \left(\frac{f_a}{f_s} n + \frac{f_b - f_a}{2N f_s} n^2 \right). \tag{2.14}$$

The last sample is taken at $(N-1)/f_s$, not at T. Its instantaneous frequency therefore does not reach f_b exactly. If the two ends of the sweep are meant to coincide with the first and last samples, $T = (N-1)/f_s$ must be defined instead. Both conventions are valid if they are documented.

A rectangular spectrum is only an approximation for certain time–bandwidth products; it is not the exact transform of the finite chirp. A smooth window reduces sidelobes at the cost of modifying the envelope, the resolution and the energy of the pulse.

Figure 2.7 sketches the translation of the sweep: each baseband frequency is visited at a different instant, and the replica at $+f_0$ preserves that order, while in the one at $-f_0$ the order is reversed.

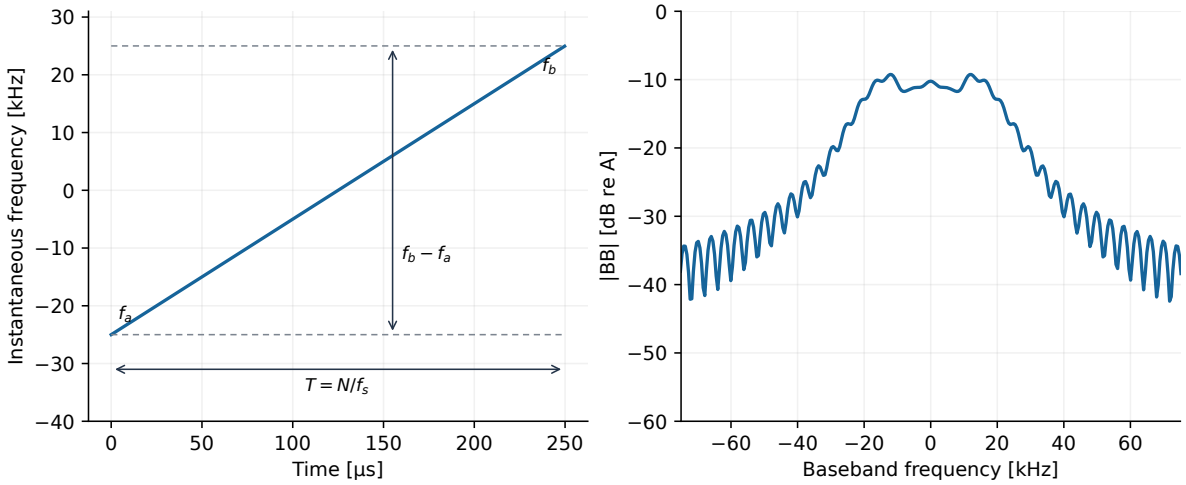

Figure 2.6: LFM chirp with $T = 250\,\mu$s and an excursion from $f_a = -25$ to $f_b = +25\,$kHz. Its spectrum shows ripple and energy outside the sweep interval due to its finite duration and window.

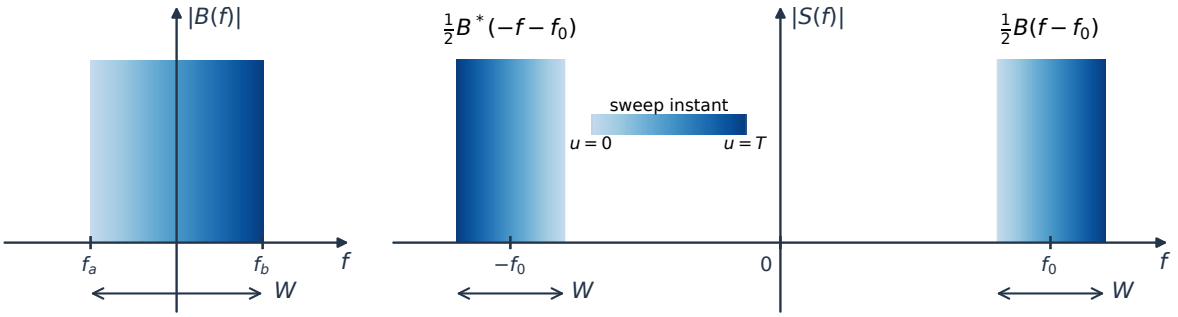

Figure 2.7: Schematic translation of a chirp of width $W = f_b - f_a$. Color indicates the instant at which each frequency is visited; the constant height is only the rectangular-spectrum approximation.

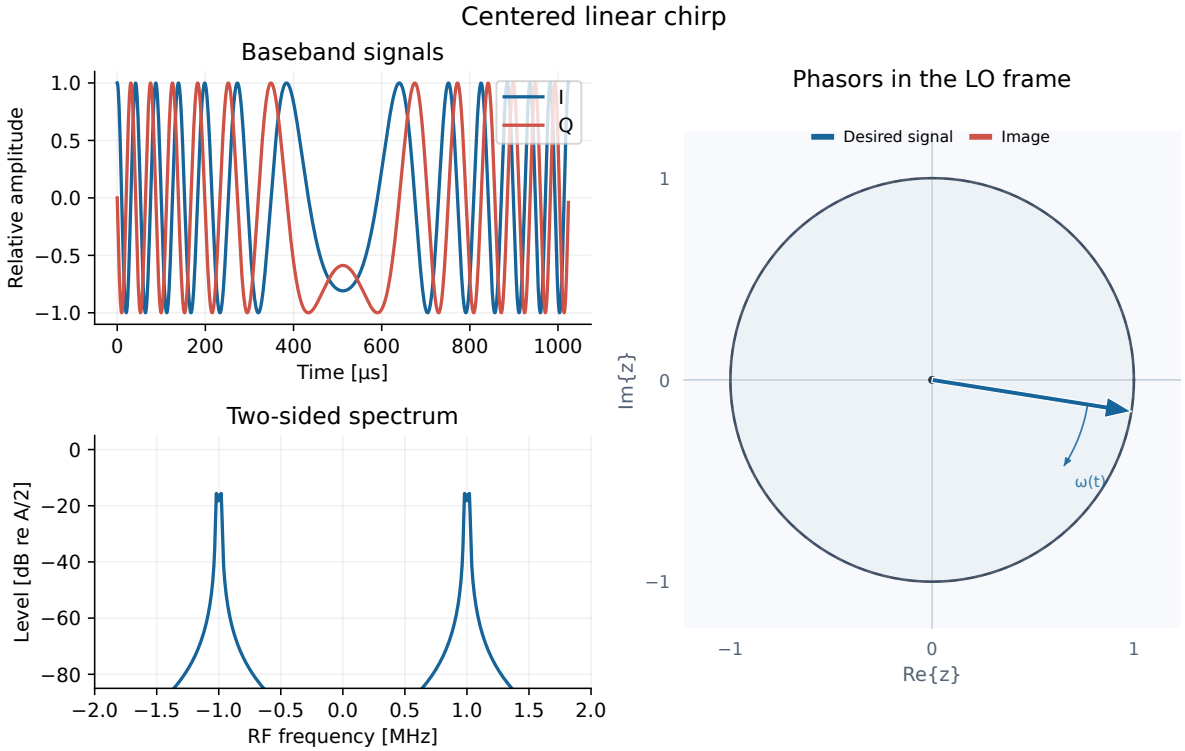

Figure 2.8: RF simulation of a centered 50 kHz chirp of 1024 μs duration, with $f_0 = 1$ MHz. The amplitude of each spectral bin depends on the duration and is referenced to $A_m/2$; it is not to be interpreted as the level of a tone.

Chapter 3

Implementation and DAC response

3.1 Generation chain

A typical implementation starts from two digital sequences, converts them with synchronized DACs, filters the sampling images and conditions their levels ahead of the mixers. The LO components must maintain the specified phase relationship. The mixer outputs are combined and may pass through an RF amplification and filtering chain [2].

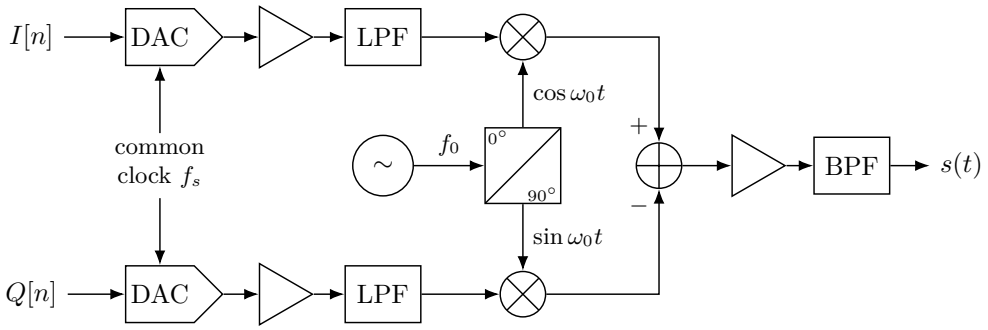

Figure 3.1: IQ modulator with DACs: conversion with a common clock, amplification, reconstruction filtering (LPF), mixing with the quadrature LO, summation and RF filtering (BPF). The signs correspond to equation (1.1); an implementation may incorporate the sign into the LO.

The quality of the balance depends on the complete chain, not only on the nominal matching of the DACs. Gains, impedances, filters and lines can introduce frequency-dependent differences. It is advisable to preserve symmetry of routing and electrical environment, and to measure the assembly under its actual load and drive conditions.

3.2 Zero-order hold and sinc

An ideal DAC with a zero-order hold holds each sample for $T_s = 1/f_s$. The causal rectangular pulse has the transform $T_s \operatorname{sinc}(fT_s)e^{-j\pi fT_s}$. After normalizing the DC gain,

$$H_{\mathrm{ZOH}}(f) = \operatorname{sinc}(f/f_s)e^{-j\pi f/f_s}, \qquad \operatorname{sinc}(x) = \frac{\sin(\pi x)}{\pi x}, \quad \operatorname{sinc}(0) = 1. \tag{3.1}$$

The complex response is distinguished from its magnitude: $|H_{\mathrm{ZOH}}(f)| = |\operatorname{sinc}(f/f_s)|$. The phase factor corresponds to a delay of $T_s/2$. The normalized definition avoids confusing the sinc of NumPy or MATLAB with the $\sin(x)/x$ convention.

At $f_s/2$, the loss is $20\log_{10}(2/\pi) = -3.9224\,\text{dB}$. It is a relative gain, not an absolute level in dBFS. The meaning of dBFS requires defining a full-scale amplitude or power. The images around multiples of f_s remain and require analog filtering; compensating the sinc roll-off does not remove them [5]. Figure 3.2(a) shows the output of a DAC for three tones of equal digital amplitude: the tones in the band of interest follow the sinc roll-off, and their images at $kf_s \pm f$ are weighted by the same envelope. The first sidelobe reaches $-13.26\,\text{dB}$ at $f \simeq 1.43 f_s$.

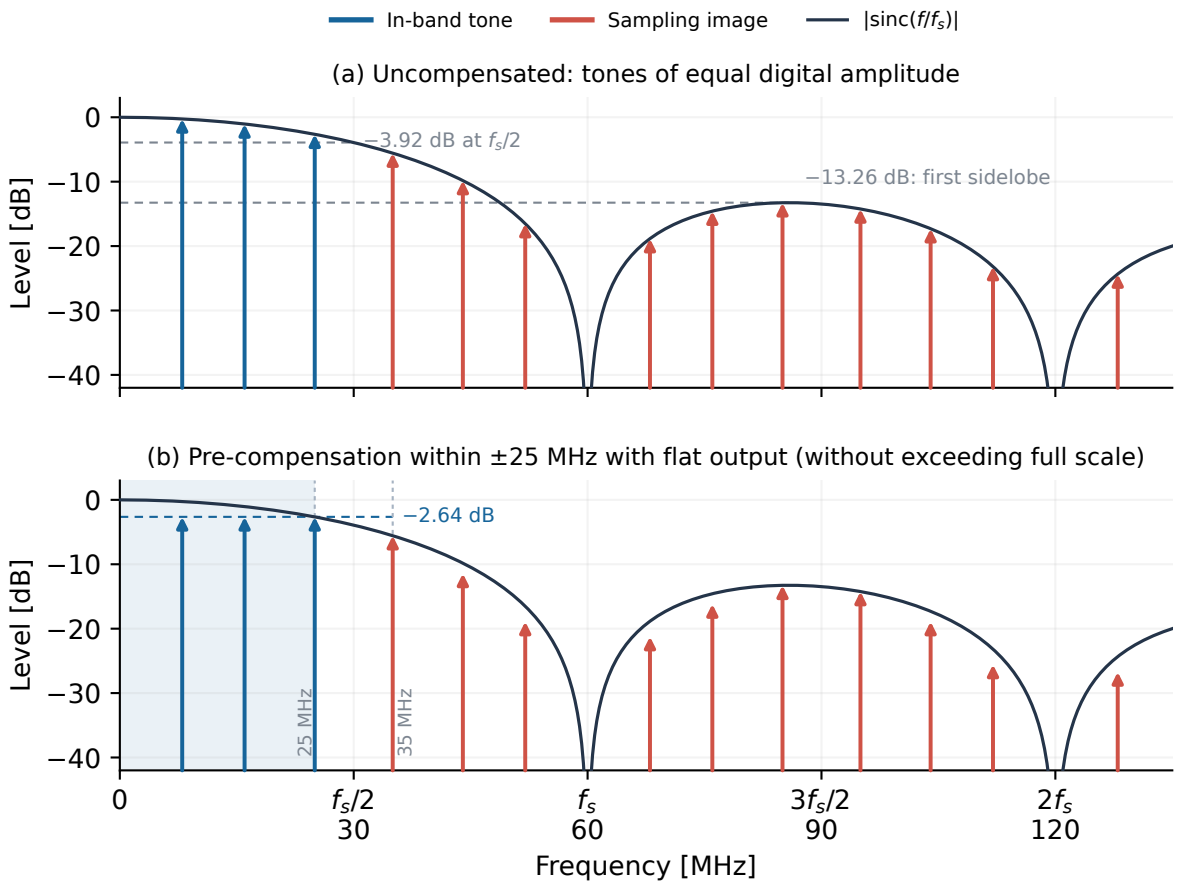

Figure 3.2: Output of a DAC with zero-order hold at $f_s = 60\,\text{MHz}$ (one-sided view of a real signal) for tones at 8, 16 and 25 MHz: (a) without compensation; (b) with amplitude pre-compensation limited to the band of interest and normalized to the band-edge level.

3.3 Compensation within the band of interest

To compensate only the magnitude, an ideal pre-equalization in the band $\mathcal{B}$ is

$$B_{\text{pre}}(f) = \frac{B(f)}{|\operatorname{sinc}(f/f_s)|}, \qquad f \in \mathcal{B}. \tag{3.2}$$

Outside that band, the gain is limited or a filter transition is applied. The inverse must not be extended to the zeros of the sinc. A complex inverse would include $e^{j\pi f/f_s}$, which represents a time advance; a causal implementation must add sufficient latency and accept a band-limited approximation.

For $f_s = 60\,\text{MHz}$ and a band of interest of 50 MHz centered at zero,

$$|H_{\text{ZOH}}(25\,\text{MHz})| \simeq 0.7379, \quad L \simeq -2.6399\,\text{dB}, \quad G_{\text{pre}} \simeq 1.3552. \tag{3.3}$$

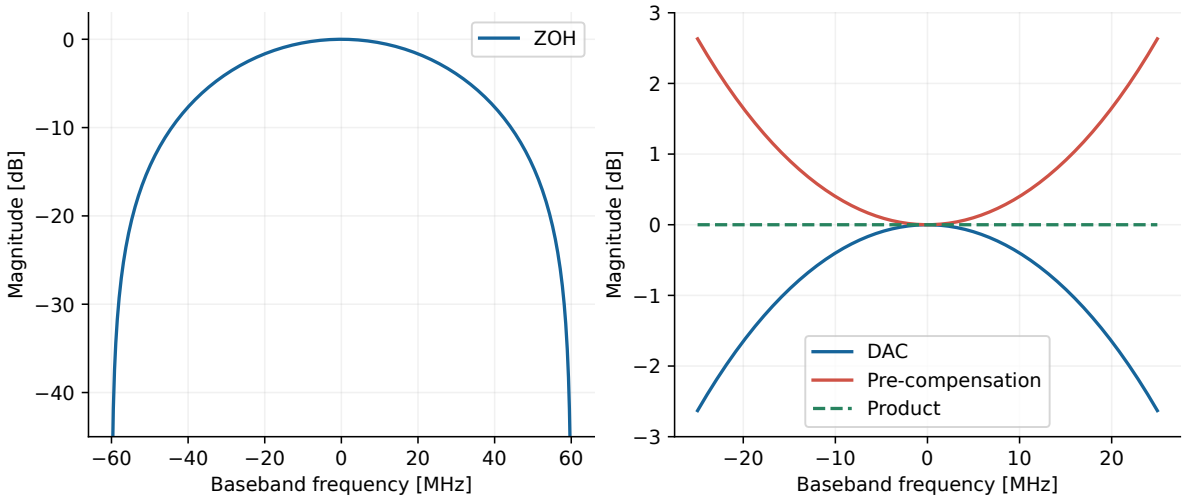

Figure 3.3: Magnitude of the zero-order hold and pre-compensation limited to ±25 MHz for $f_s = 60$ MHz.

The extra gain consumes DAC headroom. For a band-edge tone, keeping the same maximum peak requires scaling its digital amplitude down by at least the factor 1/1.3552. For multitone signals or chirps, the constraint depends on the time-domain peak of the pre-equalized signal and cannot be inferred from the maximum gain of the filter alone. Saturation, crest factor and quantization must be checked after all corrections have been applied.

Figure 3.2(b) applies that normalization by means of tables: the tones in the band of interest come out at the band-edge level, −2.64 dB, without exceeding full scale. The images are scaled together with each tone; their rejection depends on the reconstruction filter, whose transition must lie between 25 and 35 MHz in this example.

A filter common to I and Q corrects a common response. If the branches have different responses, the pre-equalization must include that difference: an identical sinc correction does not remove the differential imbalance.

Chapter 4

DC offsets and carrier leakage

4.1 Offset model

With offsets referred to the baseband inputs,

$$b_O(t) = b(t) + O_I + jO_Q = b(t) + Oe^{j\theta_O}, \tag{4.1}$$

$$O = \sqrt{O_I^2 + O_Q^2}, \qquad \theta_O = \operatorname{atan2}(O_Q, O_I). \tag{4.2}$$

The real output is

$$s_O(t) = s(t) + O_I \cos\omega_0 t - O_Q \sin\omega_0 t = s(t) + O\cos(\omega_0 t + \theta_O). \tag{4.3}$$

The offset produces a component exactly at f_0. In the rotating LO frame it shifts the center of the envelope trajectory. By itself, it does not change the ratio between the signal and the image of the tone. Figure 4.1 illustrates this with an exaggerated offset: the static vector O shifts the center of the circle, and the signal phasor rotates around the new center. In the spectrum (figure 4.2), the offset adds a line at baseband DC that is translated to $\pm f_0$ with amplitude $O/2$, both for a generic envelope and for a tone.

For a desired signal of amplitude A_m, the leakage level is

$$L_{\mathrm{LO}} = 20\log_{10}(O/A_m) \quad [\mathrm{dBc}]. \tag{4.4}$$

If $O = 0.05A_m$, the result is $-26.02\,\mathrm{dBc}$. The example in figure 4.3 uses $O_I = 0.04A_m$ and $O_Q = 0.03A_m$, whose magnitude is precisely $0.05A_m$.

The physical leakage may include direct coupling from the LO to the RF output, in addition to the conversion of offsets. Both contributions can be added vectorially. A DC correction can cancel the observable sum if it has the required range and two independent adjustment directions [4].

4.2 Digital and analog compensation

Digital compensation adds constants to I and Q. It is flexible and allows adjustments to be stored per mode, but it reduces the headroom available before full scale is reached. Analog correction introduces a DC adjustment after the signal DACs; it preserves their digital range, although the range and linearity of the analog chain still limit the result. Both methods can be combined; figure 4.4 shows the two injection points.

In the ideal model, $O_I^{\mathrm{corr}} = -O_I$ and $O_Q^{\mathrm{corr}} = -O_Q$ suffice. In an implementation, the relationship between the correction code and the leakage vector depends on the gains and phases of the branches. If these change with the LO, temperature or level, the optimum adjustment changes as well.

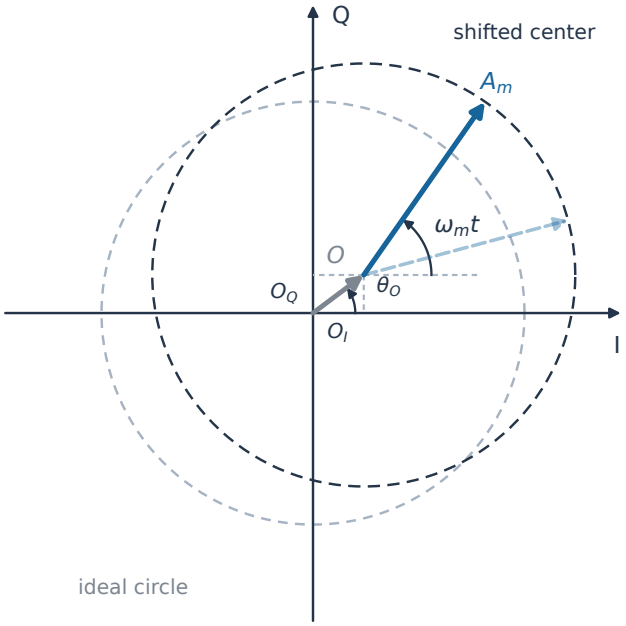

Figure 4.1: Phasor representation of an offset $O = 0.3A_m$ with $\theta_O = 36.9°$, exaggerated for readability. The vector O is static in the LO frame and shifts the center of the trajectory.

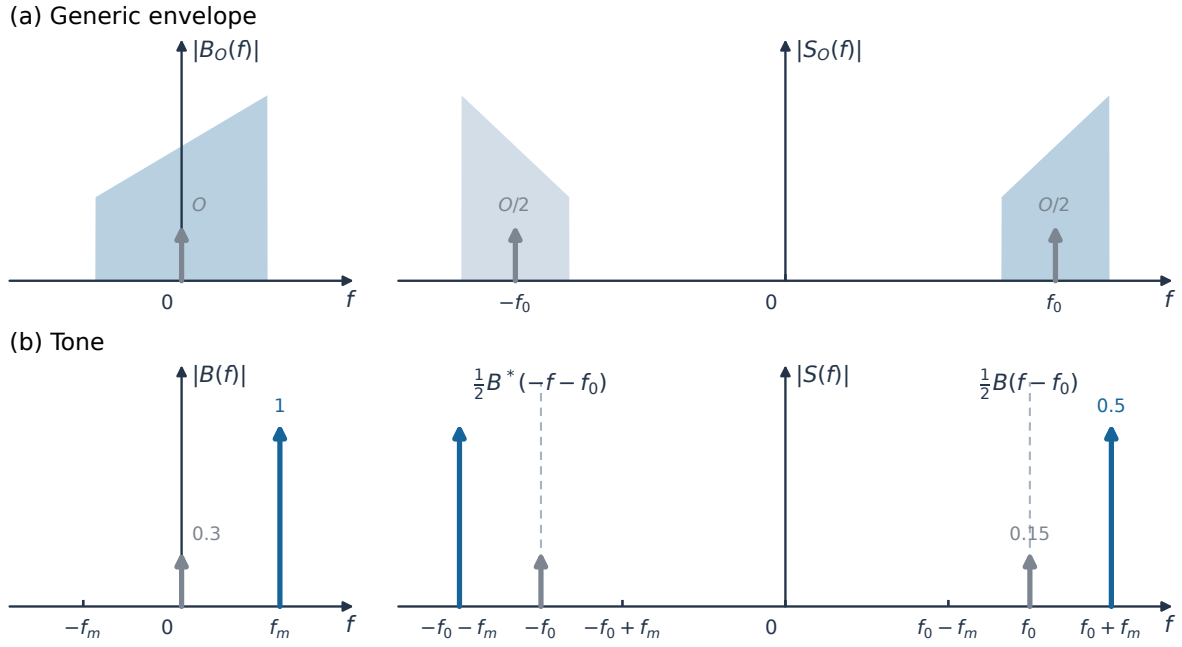

Figure 4.2: Spectra with a DC offset $O = 0.3A_m$: (a) generic envelope; (b) tone. The leakage appears exactly at f_0 and at its replica $-f_0$.

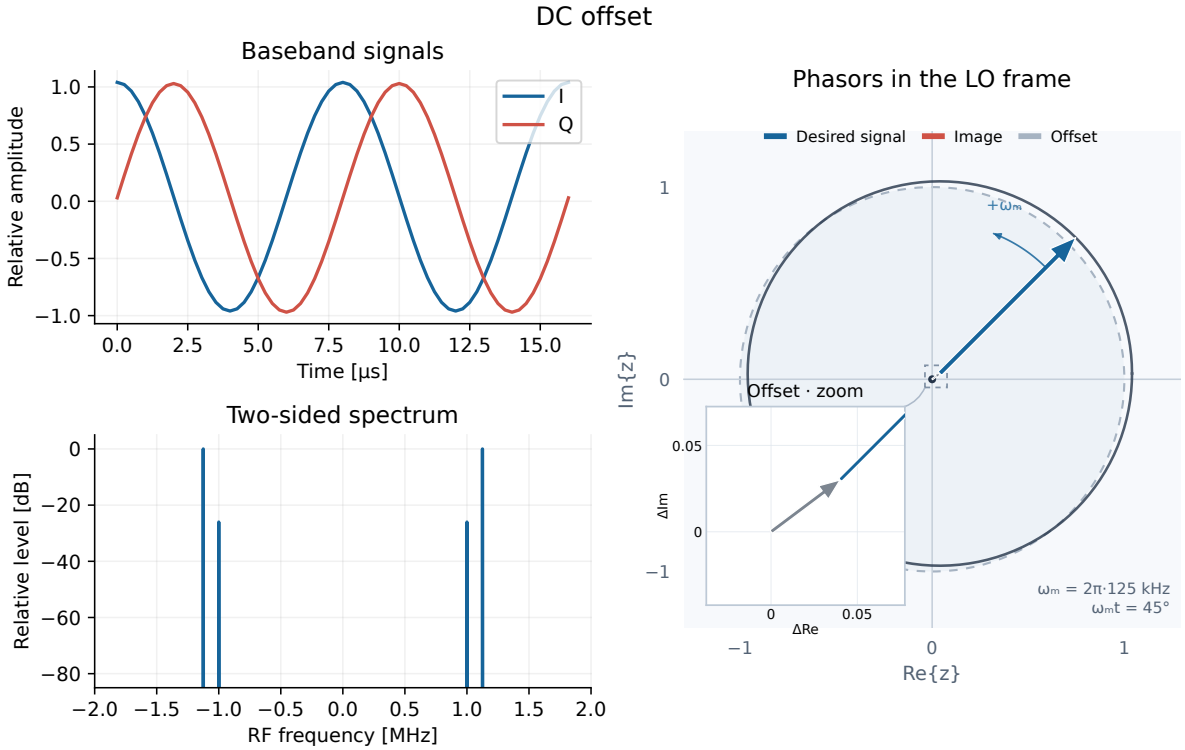

Figure 4.3: Offsets $O_I = 0.04$ and $O_Q = 0.03$ for $A_m = 1$. The RF component at f_0 lies at $-26.02\,\mathrm{dBc}$.

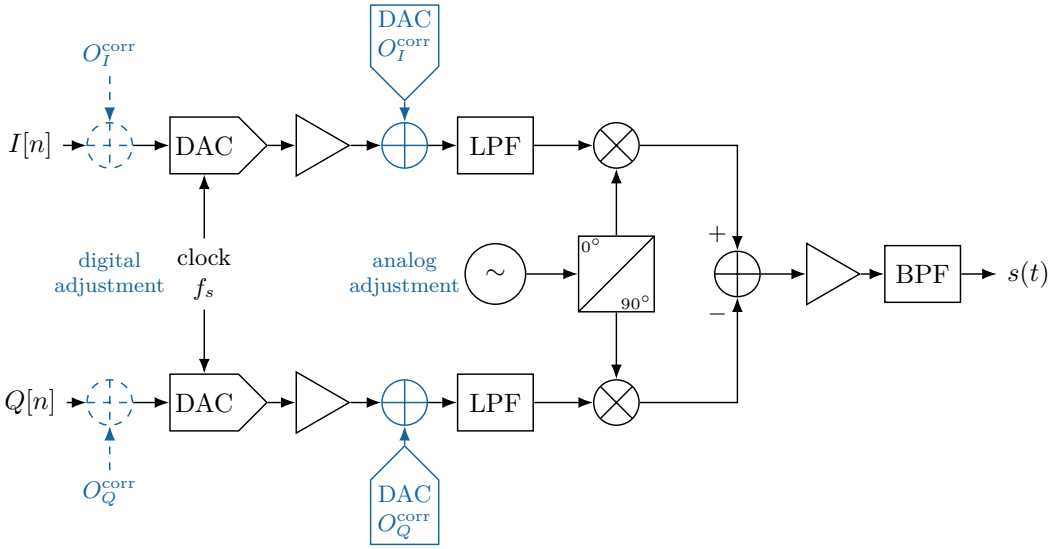

Figure 4.4: Offset correction: digital adjustment added to the sequences before the DACs (dashed line) or analog adjustment through auxiliary DACs after the signal DACs.

4.3 Searching for the minimum

Using a tone offset from the LO so that the leakage can be resolved spectrally:

1. Measure the leakage power at f_0 with stable range and resolution.
2. Sweep the I adjustment, locate its minimum and refine the step.
3. Repeat for Q while keeping the previous I adjustment.
4. Alternate between both adjustments until the minimum stops improving.
5. Confirm that the desired signal is not clipped, and record the codes, the temperature, the LO and the measurement uncertainty.

In the linear model, the leakage power is a quadratic function of the two adjustments. If the directions are not orthogonal, a single pass over each channel does not guarantee the global minimum. Near the noise floor, the measurement can no longer distinguish small changes; zero leakage should not be reported on the basis of an instrument-limited reading.

Chapter 5

Gain imbalance

5.1 General model with a conjugate component

With constant real gains,

$$b_G(t) = G_I I(t) + jG_Q Q(t) = \alpha_G b(t) + \beta_G b^*(t), \tag{5.1}$$

where

$$\alpha_G = \frac{G_I + G_Q}{2}, \qquad \beta_G = \frac{G_I - G_Q}{2}. \tag{5.2}$$

This expression holds for any envelope, not only for a tone. The conjugate term produces a mirrored version of its spectrum. For frequency-dependent gains, the constants are replaced by LTI responses, as developed in chapter 9.

5.2 Tone and elliptical trajectory

For $b(t) = A_m e^{j\omega_m t}$,

$$s_G(t) = A_m \frac{G_I + G_Q}{2} \cos[(\omega_0 + \omega_m)t] + A_m \frac{G_I - G_Q}{2} \cos[(\omega_0 - \omega_m)t]. \tag{5.3}$$

The desired amplitude is $A_{mG} = A_m(G_I + G_Q)/2$ and the image coefficient is $A_{BL} = A_m(G_I - G_Q)/2$. If the latter is negative, it is interpreted as a phase shift of π; its physical amplitude is $|A_{BL}|$.

The trajectory $G_I A_m \cos\omega_m t + jG_Q A_m \sin\omega_m t$ is an ellipse with axes aligned with I and Q. It can be decomposed into two vectors rotating at $+f_m$ and $-f_m$ in the LO frame. Figure 5.1 shows both interpretations for $G_I = 1.2$ and $G_Q = 0.7$: in (a), the semi-axes of the ellipse are $G_I A_m$ and $G_Q A_m$; in (b), the same trajectory is the sum of $De^{j\omega_m t}$, with magnitude $|D| = 0.95A_m$, and $Ee^{-j\omega_m t}$, with magnitude $0.25A_m$. Image cancellation requires equal gains, but the nominal amplitude additionally requires their average to be one.

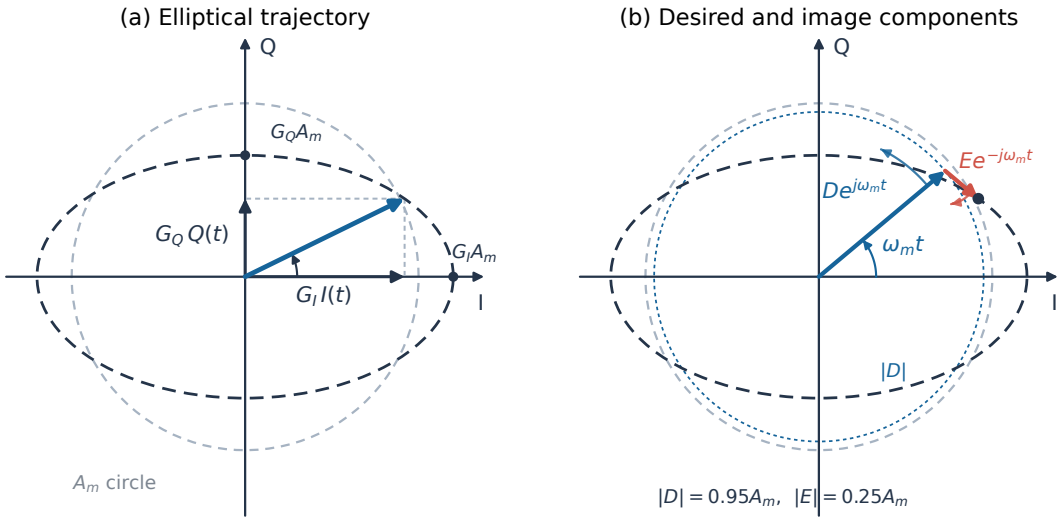

Figure 5.1: Gain imbalance with $G_I = 1.2$ and $G_Q = 0.7$: (a) elliptical trajectory and projections $G_I I(t)$ and $G_Q Q(t)$; (b) decomposition into a desired component and an image rotating in opposite directions.

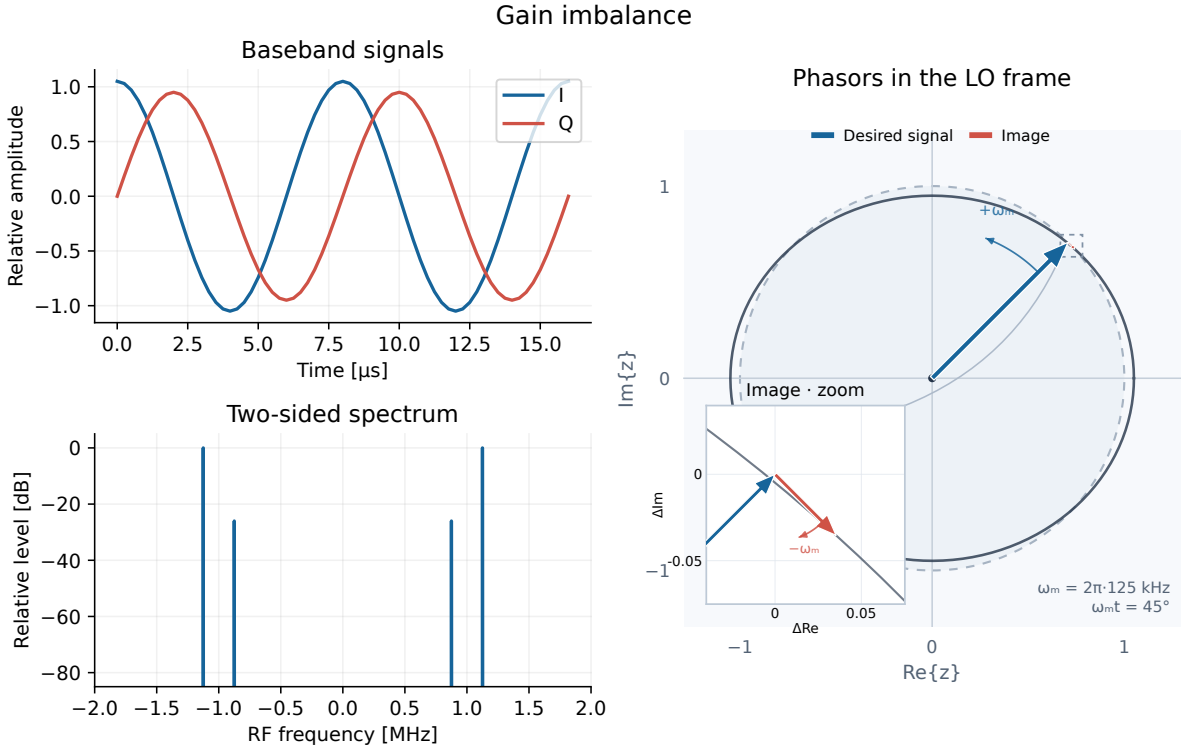

Figure 5.2: Case $G_I = 1.05$, $G_Q = 0.95$: unit desired amplitude and an image of amplitude 0.05, equivalent to -26.02 dBc.

5.3 Metrics and examples

$$\frac{P_{\text{img}}}{P_{\text{des}}} = \left|\frac{G_I - G_Q}{G_I + G_Q}\right|^2, \tag{5.4}$$

$$L_{\text{img}} = 20\log_{10}\left|\frac{G_I - G_Q}{G_I + G_Q}\right|, \tag{5.5}$$

$$G_{\text{des,dB}} = 20\log_{10}\left|\frac{G_I + G_Q}{2}\right|. \tag{5.6}$$

The two metrics represent different constraints: minimizing the image and preserving the desired amplitude. Decomposing an amplitude change into two terms at the same frequency does not create a third, independent spectral line. Figure 5.3 shows this for the second row of table 5.1: the desired line falls below the nominal level (dashed line) and a single image line appears at $f_0 - f_m$.

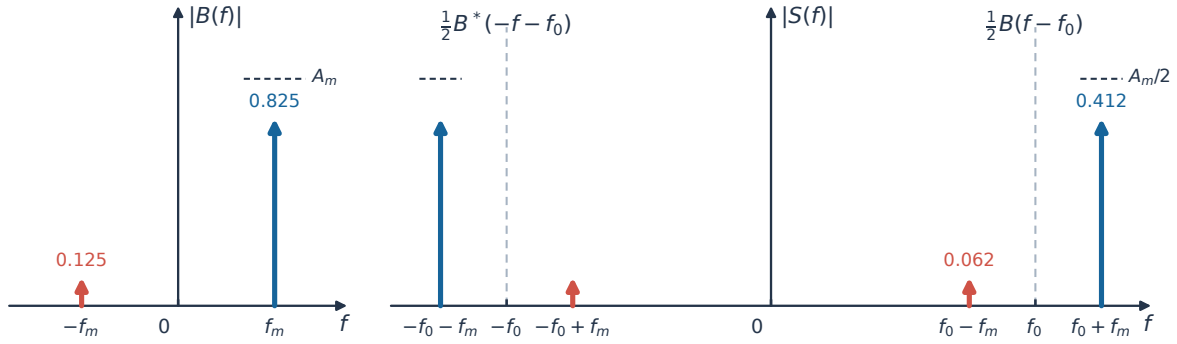

Figure 5.3: Line spectrum with $G_I = 0.95$ and $G_Q = 0.70$: $|D| = 0.825A_m$ and image $|E| = 0.125A_m$, i.e., -16.39 dBc. The dashed line indicates the nominal level.

Table 5.1: Gain imbalance examples.

G_I	G_Q	$\lvert D\rvert/A_m$	Image [dBc]	Desired-signal gain [dB]
1.05	0.95	1.000	−26.02	0.00
0.95	0.70	0.825	−16.39	−1.67
1.20	0.70	0.950	−11.60	−0.45

5.4 Compensation and resolution limit

If both gains are known and nonzero, the factors $g_I = G_{\text{obj}}/G_I$ and $g_Q = G_{\text{obj}}/G_Q$ can be applied. The common target value is chosen to avoid saturation; amplifying the weaker branch may consume headroom or raise its noise. Attenuating the stronger branch is usually simpler, but it lowers the overall level.

If $G_I = 1 + \epsilon$ and $G_Q = 1 - \epsilon$, then $|E/D| = |\epsilon|$. A rejection of 40 dB requires $|\epsilon| \leq 0.01$ when this is the only error. If there is also a phase error, adjusting the gains until they are equal does not guarantee that rejection. The joint calibration must be evaluated on the complete RF output.

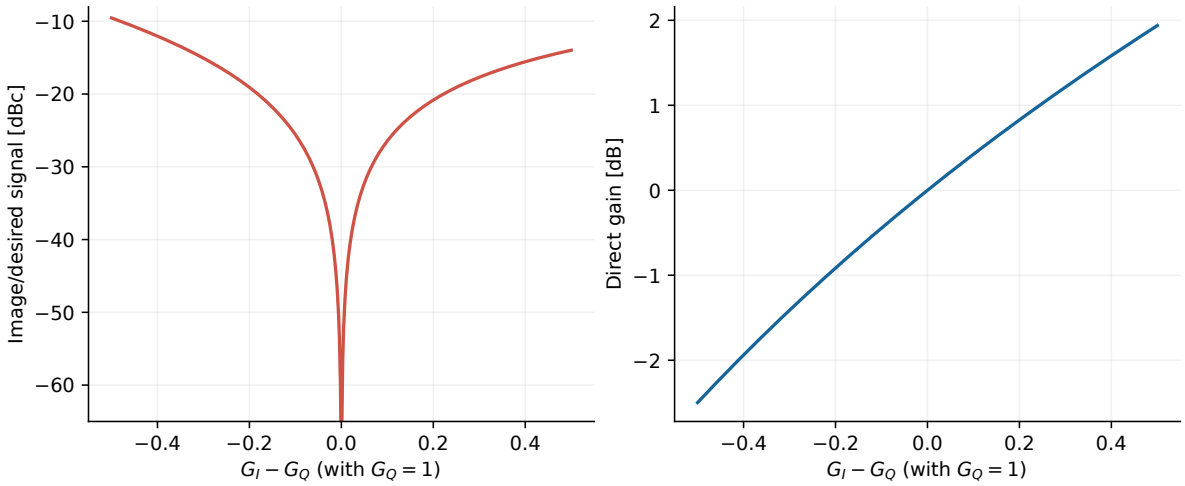

Figure 5.4: Image level and desired-signal gain as $G_I - G_Q$ varies, with $G_Q = 1$. The image reference is the actual desired signal.

Chapter 6

Local oscillator quadrature error

6.1 Mixer model

If the LO components exhibit phase errors ϕ_I and ϕ_Q,

$$s_\phi(t) = I(t)\cos(\omega_0 t + \phi_I) - Q(t)\sin(\omega_0 t + \phi_Q). \tag{6.1}$$

The errors are deviations from the nominal phases; they are not the absolute phases of two identical carriers. We define

$$\Delta\phi = \phi_I - \phi_Q, \qquad \bar{\phi} = (\phi_I + \phi_Q)/2. \tag{6.2}$$

The physical separation between the carriers is $90^\circ + \phi_Q - \phi_I$. Ideal quadrature corresponds to $\Delta\phi = 0$, not to a 90° difference between the errors. Figure 6.1 places these errors at the outputs of the LO phase splitter.

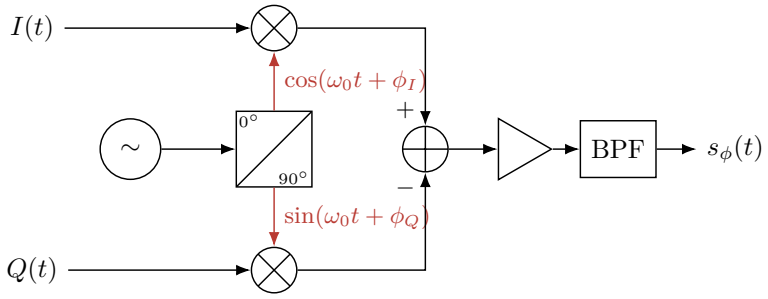

Figure 6.1: Quadrature error in the local oscillator: the splitter outputs exhibit deviations ϕ_I and ϕ_Q from their nominal phases.

An equivalent envelope referred to an ideal LO is

$$z_\phi(t) = e^{j\phi_I} I(t) + j e^{j\phi_Q} Q(t) = \alpha_\phi b(t) + \beta_\phi b^*(t), \tag{6.3}$$

$$\alpha_\phi = e^{j\bar{\phi}}\cos(\Delta\phi/2), \qquad \beta_\phi = j e^{j\bar{\phi}}\sin(\Delta\phi/2). \tag{6.4}$$

Taking $\mathrm{Re}\{z_\phi e^{j\omega_0 t}\}$ recovers equation (6.1) exactly. This formulation keeps the real output and the complex representation separate, and avoids interpreting an exponential as if it were directly the measurable RF voltage.

6.2 Tone, image and common phase

For $b(t) = A_m e^{j\omega_m t}$,

$$\begin{aligned} s_\phi(t) &= A_m \cos(\Delta\phi/2)\cos[(\omega_0+\omega_m)t + \bar{\phi}] \\ &\quad + A_m \sin(\Delta\phi/2)\cos[(\omega_0-\omega_m)t + \bar{\phi} + \pi/2]. \end{aligned} \tag{6.5}$$

The sign of the sine can be absorbed into an additional phase of π to express positive amplitudes. The common phase $\bar{\phi}$ rotates the envelope, while the phase difference produces the image and distorts its trajectory. In figure 6.2(a), the effective axes $e^{j\phi_I}$ and $je^{j\phi_Q}$ are no longer orthogonal and the trajectory becomes a tilted ellipse. In (b), the same trajectory is decomposed into the desired component, rotated by $\bar{\phi}$, and the image. Figure 6.3 indicates the magnitudes and phases of both lines.

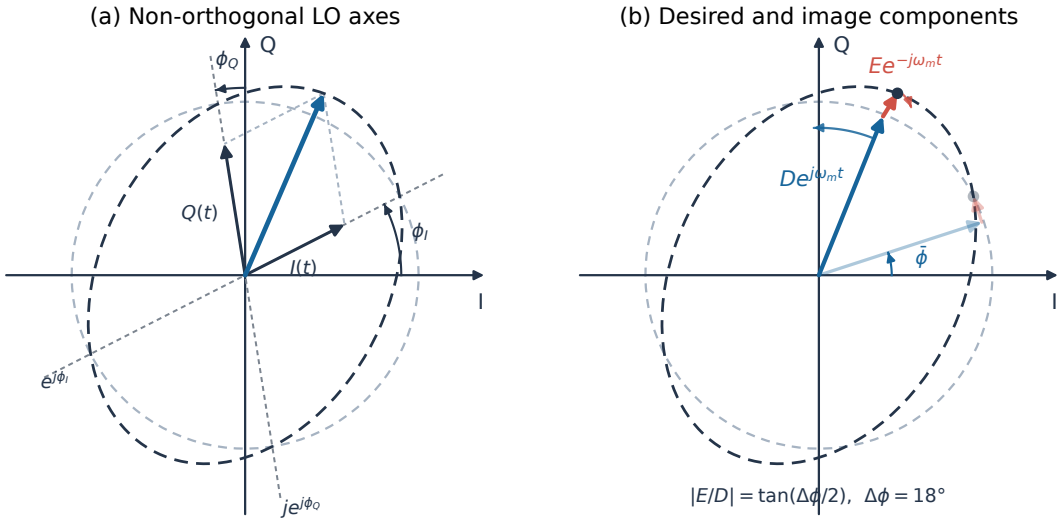

Figure 6.2: Quadrature error with $\phi_I = 27°$ and $\phi_Q = 9°$: (a) non-orthogonal effective axes; (b) desired and image components. The major axis of the ellipse does not coincide with the I and Q axes.

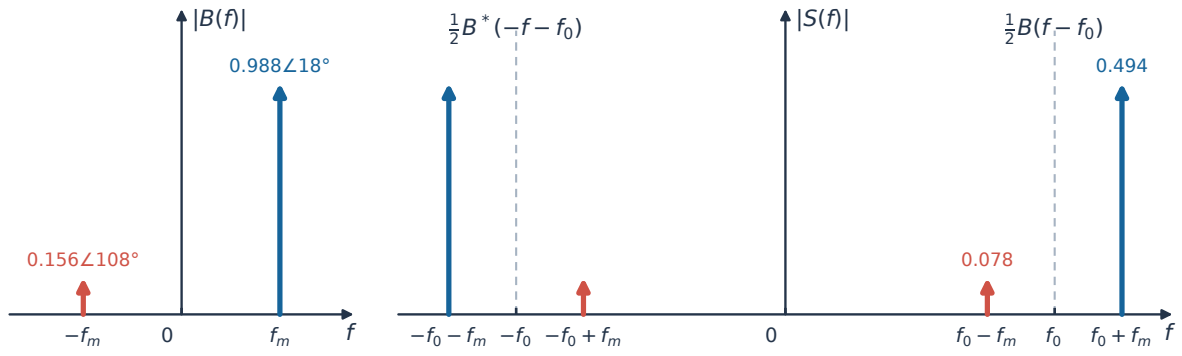

Figure 6.3: Line spectrum for the case of figure 6.2: the desired line has phase $\bar{\phi} = 18°$ and the image has phase $\bar{\phi} + 90° = 108°$, with magnitudes $\cos(\Delta\phi/2)$ and $\sin(\Delta\phi/2)$.

$$L_{\text{img}} = 20\log_{10}|\tan(\Delta\phi/2)|, \qquad \text{IRR} = -20\log_{10}|\tan(\Delta\phi/2)|. \tag{6.6}$$

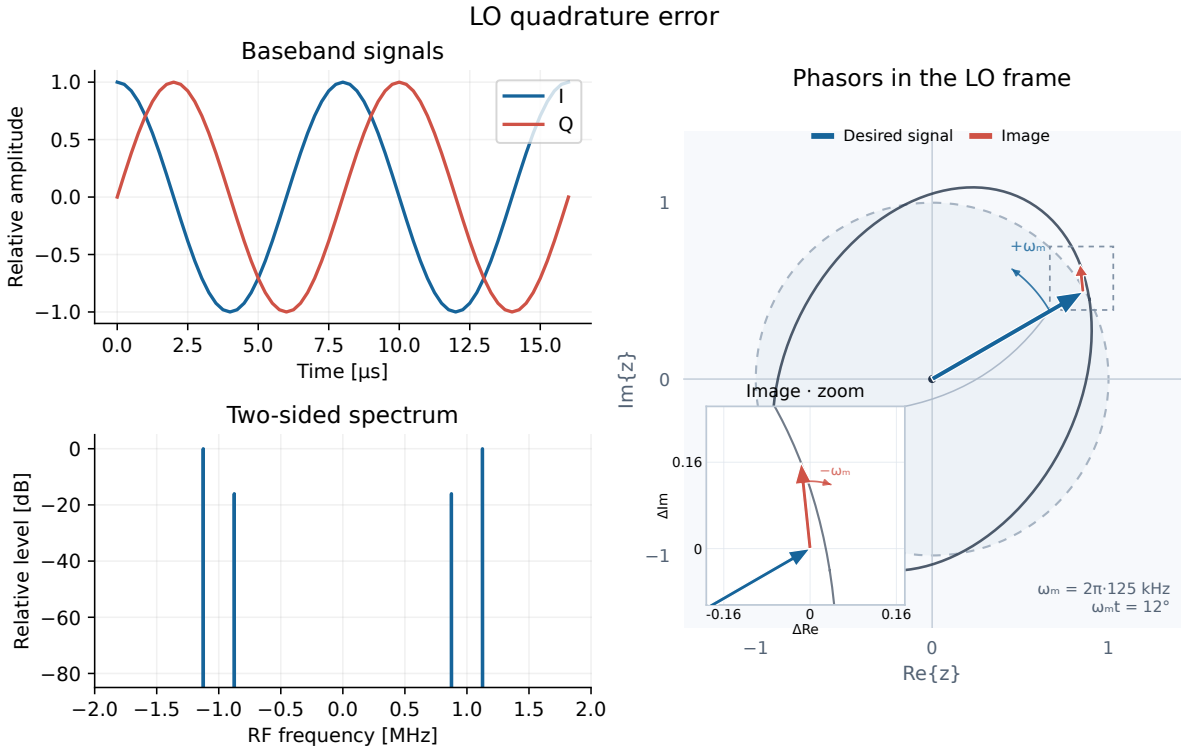

Figure 6.4: Errors $\phi_I = 27°$ and $\phi_Q = 9°$: $\Delta\phi = 18°$, a common rotation of 18° and an image at approximately -16.01 dBc.

For $|\Delta\phi| \ll 1$, the amplitude ratio is approximately $|\Delta\phi|/2$. An error of 1° produces approximately -41.18 dBc when no other non-idealities are present. If $\phi_I = \phi_Q$, the image vanishes but the common phase rotation remains.

6.3 Simultaneous gain and phase errors

If gains G_I, G_Q are also present, the coefficients are

$$\alpha = \frac{G_I e^{j\phi_I} + G_Q e^{j\phi_Q}}{2}, \qquad \beta = \frac{G_I e^{j\phi_I} - G_Q e^{j\phi_Q}}{2}. \tag{6.7}$$

The power ratio becomes

$$\frac{P_{\text{img}}}{P_{\text{des}}} = \frac{G_I^2 + G_Q^2 - 2G_I G_Q \cos\Delta\phi}{G_I^2 + G_Q^2 + 2G_I G_Q \cos\Delta\phi}. \tag{6.8}$$

Phase and gain jointly contribute to the rejection. A phase improvement may be almost invisible if the gain error dominates, and vice versa. Error levels in dB must not be added as if they were independent powers: the contributions to the image are complex and coherent.

The correction can be performed through LO adjustments or by digitally combining the I and Q signals before the DACs. A simple common complex rotation does not correct the loss of orthogonality: this requires a transformation that includes the conjugate term or its equivalent real matrix, as in chapter 9.

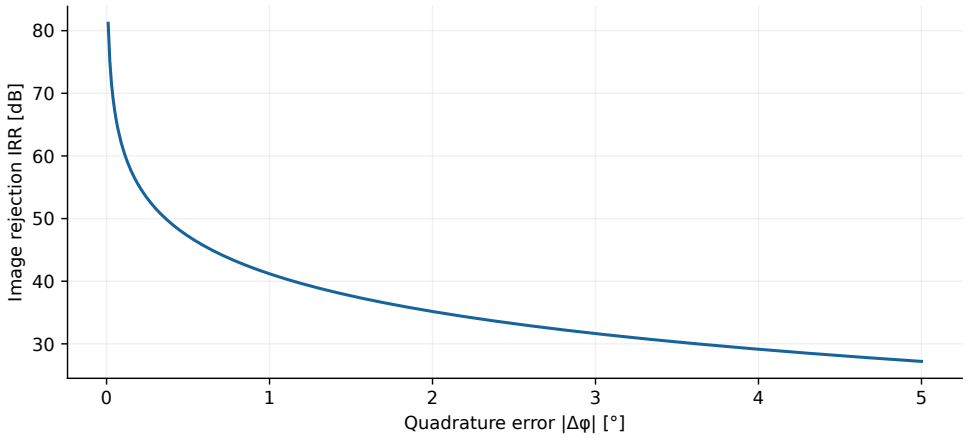

Figure 6.5: Image rejection for quadrature errors between 0.01° and 5°. At zero, the ideal model has infinite rejection; a physical system is limited by other errors.

Chapter 7

Coupling between baseband branches

7.1 LTI model and the need for an equivalent circuit

Coupling may arise from parasitic capacitances, mutual inductance, shared supply impedances or return paths. Its frequency dependence is not determined merely by naming the mechanism: the excitation, the loads and the source impedances all play a role. The general description for two channels is

$$\begin{bmatrix} I_{\mathrm{sal}}(f) \\ Q_{\mathrm{sal}}(f) \end{bmatrix} = \begin{bmatrix} H_{II}(f) & H_{IQ}(f) \\ H_{QI}(f) & H_{QQ}(f) \end{bmatrix} \begin{bmatrix} I_f(f) \\ Q_f(f) \end{bmatrix}. \tag{7.1}$$

The transfer functions are obtained from a circuit or from a measurement. For real physical channels, $H_{xy}(-f) = H^*_{xy}(f)$. Their implementation in the FFT domain must preserve this symmetry. Figure 7.1 represents the matrix as a two-input, two-output network located before the mixers.

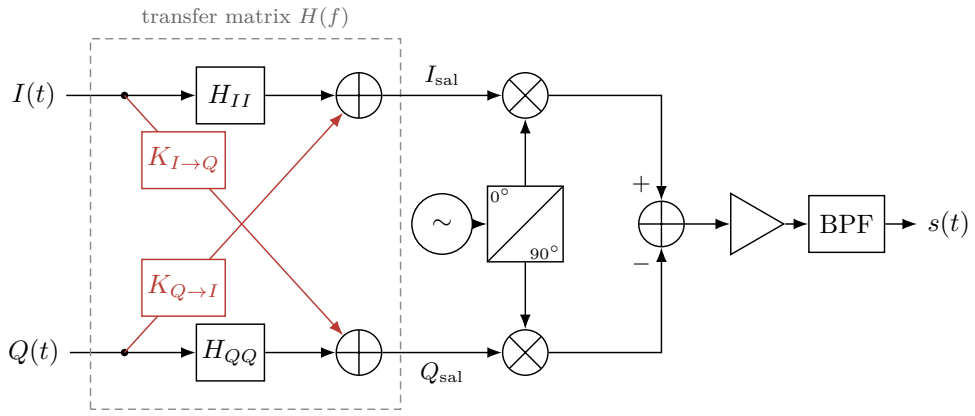

Figure 7.1: Coupling between baseband branches represented by the matrix $H(f)$ of equation (7.1). The cross-coupling terms are $K_{I\to Q} = H_{QI}$ and $K_{Q\to I} = H_{IQ}$.

A capacitor obeys $i_C = C\, dv_C/dt$. A mutual inductance produces $v_{\mathrm{ind}} = \pm M\, di/dt$, with the sign depending on the orientation of the windings or on the terminal convention [6]. Therefore, an integrating term applied to a baseband voltage does not by itself constitute a universal model of inductive coupling. At DC, a constant current induces no voltage, but this does not imply that the mutual inductance M is zero.

If an empirical approximation $K(\omega) = k_0 + k_1 j\omega + k_{-1}/(j\omega)$ is used in a band that excludes zero, its coefficients and validity must be confined to that band. The approximation is not extended to DC, nor is each term attributed to a physical mechanism without deriving the circuit. The

correct phase conversions for $\omega > 0$ are

$$j\omega e^{-j\omega\tau} = \omega e^{-j(\omega\tau-\pi/2)}, \tag{7.2}$$

$$\frac{e^{-j\omega\tau}}{j\omega} = \frac{1}{\omega} e^{-j(\omega\tau+\pi/2)}. \tag{7.3}$$

7.2 Asymmetric cross-coupling

If the direct responses are unity and the cross-coupling terms are $K_{Q\to I}$ and $K_{I\to Q}$, one obtains

$$\begin{aligned} B_{\text{sal}}(f) = &\left[1 + \frac{j}{2}(K_{I\to Q} - K_{Q\to I})\right] B(f) \\ &+ \frac{j}{2}(K_{I\to Q} + K_{Q\to I}) B^*(-f). \end{aligned} \tag{7.4}$$

The responses are evaluated at the output frequency f. The average of the cross-coupling terms produces an image, while their difference modifies the direct component. Reduction to a pure image explicitly requires $K_{I\to Q} = K_{Q\to I} = K$:

$$B_{\text{sal}}(f) = B(f) + jK(f)B^*(-f). \tag{7.5}$$

The equality does not follow merely from the two channels being close to each other or from the presence of a reciprocal element: the impedances and gains of the chain can make the overall transfer functions differ.

For a tone, symmetric cross-coupling yields $D = A_m$ and $E = jK(-\omega_m)A_m = jK^*(\omega_m)A_m$. Figure 7.2 compares the three terms of the empirical approximation with equal magnitude. A constant term tilts the ellipse to 45°; a term proportional to $j\omega$ produces an image in phase with the signal and elongates the trajectory along the I axis; a term proportional to $1/(j\omega)$ produces an image in antiphase and elongates it along the Q axis. If they coexist, their relative weight changes with frequency and the major axis rotates. This dependence distinguishes cross-coupling from an LO quadrature error, whose tilt does not depend on f_m. This interpretation holds for the approximation fitted within a band; by itself, it does not identify the physical mechanism.

Swapping I and Q without filtering produces $Q + jI = jb^*$. For a tone, conjugation reverses the direction of rotation and the factor j introduces +90° in the complex plane (figure 7.4). The negative rotation refers to baseband; the RF image is still located at $f_0 - f_m$.

7.3 Symmetric capacitive circuit

Consider two sources V_{SI}, V_{SQ}, each with series resistance R_S and a load R_L to ground. A capacitance C_M connects the nodes V_I, V_Q. The resistances are real and equal in both branches, and the lumped model applies as long as the lines do not require a distributed description.

With $Y_S = 1/R_S$, $Y_L = 1/R_L$ and $Y_C = j\omega C_M$, the nodal equations are

$$\begin{bmatrix} Y_S + Y_L + Y_C & -Y_C \\ -Y_C & Y_S + Y_L + Y_C \end{bmatrix} \begin{bmatrix} V_I \\ V_Q \end{bmatrix} = Y_S \begin{bmatrix} V_{SI} \\ V_{SQ} \end{bmatrix}. \tag{7.6}$$

Defining

$$R = R_S \parallel R_L, \quad \tau_C = RC_M, \quad x = \omega\tau_C, \quad a = \frac{R_L}{R_S + R_L}, \tag{7.7}$$

the solution is

$$\begin{bmatrix} V_I \\ V_Q \end{bmatrix} = \begin{bmatrix} H_D & H_C \\ H_C & H_D \end{bmatrix} \begin{bmatrix} V_{SI} \\ V_{SQ} \end{bmatrix}, \qquad H_D = a\frac{1+jx}{1+2jx}, \quad H_C = a\frac{jx}{1+2jx}. \tag{7.8}$$

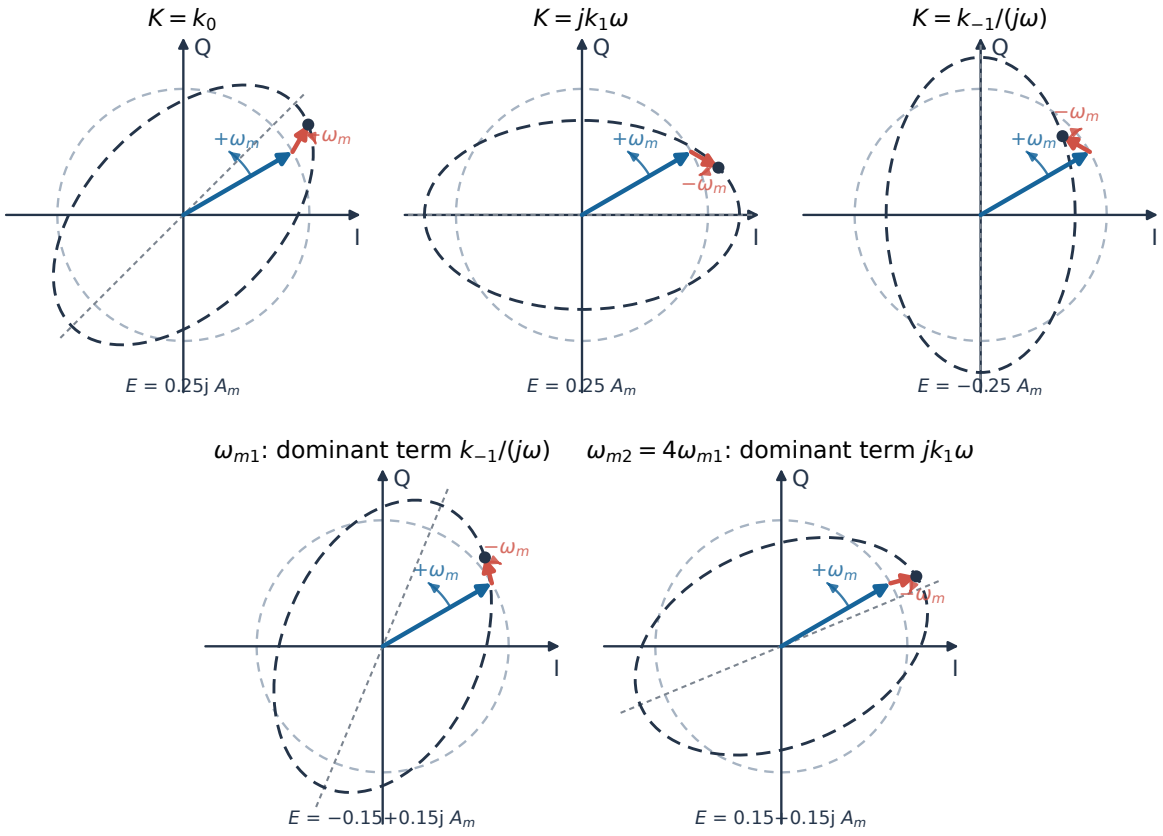

Figure 7.2: Trajectories for symmetric cross-coupling $B_{\text{sal}} = B + jKB^*(-f)$ with $|K| = 0.25$. Top row: constant, derivative and integrating terms. Bottom row: $K = 0.15 + 0.1j\omega + 0.1/(j\omega)$ at two normalized frequencies, $\omega_{m1} = 0.5$ and $\omega_{m2} = 2$. The dotted line indicates the major axis.

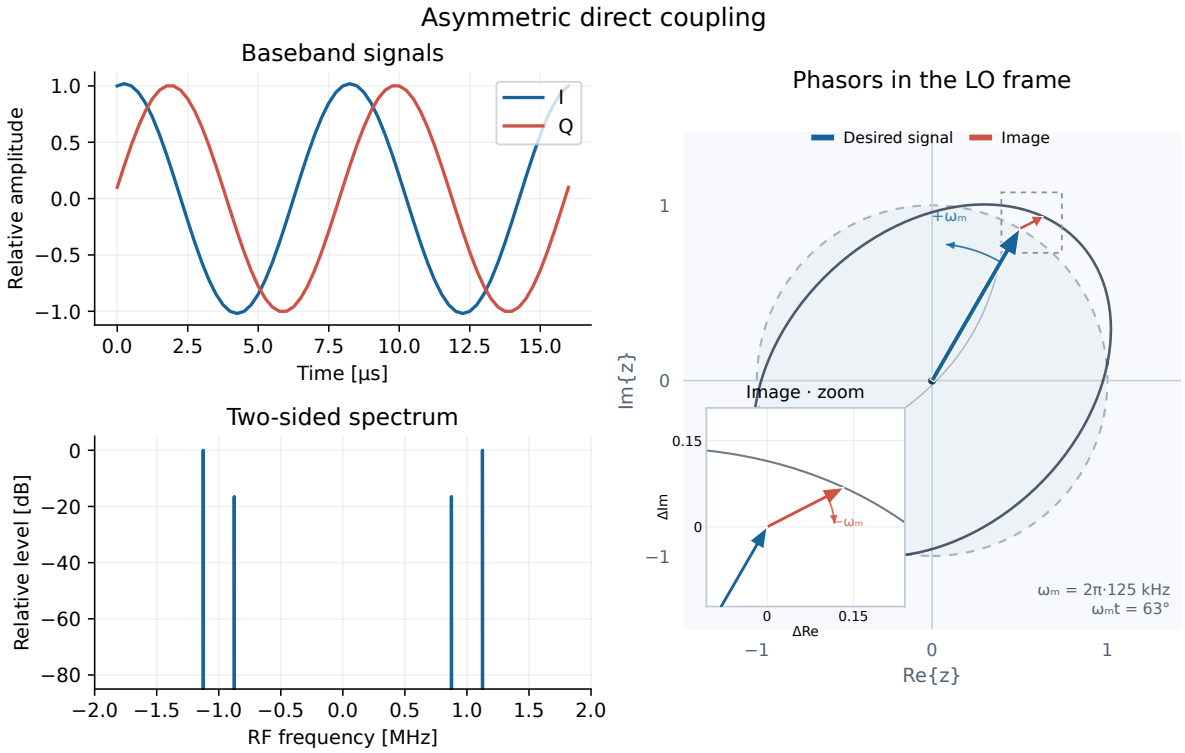

Figure 7.3: Unequal direct cross-coupling terms: $K_{I\to Q} = 0.1$ and $K_{Q\to I} = 0.2$. The direct coefficient is $1 - 0.05j$ and the image coefficient is $0.15j$.

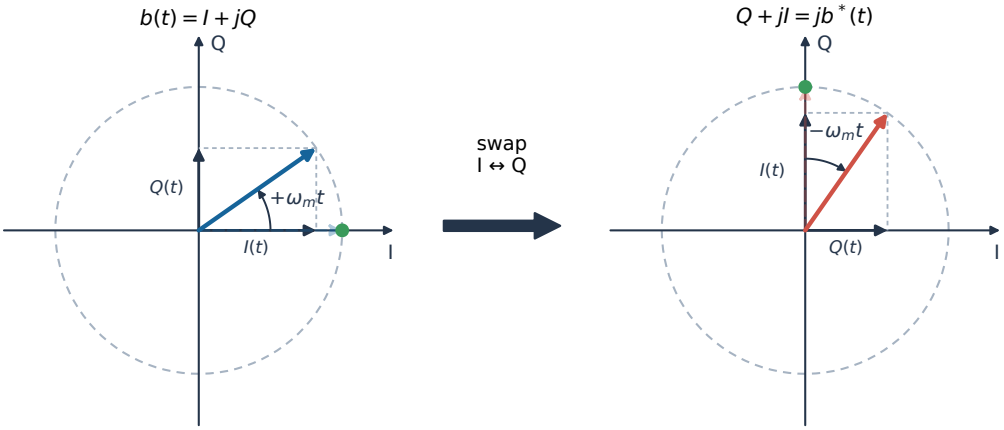

Figure 7.4: Swapping of the I and Q signals: the tone $b(t) = A_m e^{j\omega_m t}$ becomes $jb^*(t)$, which starts at 90° (green dot) and rotates in the negative direction.

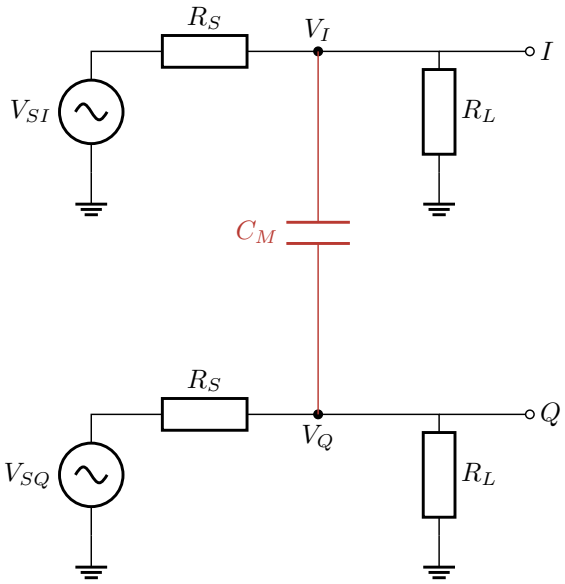

Figure 7.5: Lumped circuit of capacitive coupling between symmetric branches. When an ideal voltage source is deactivated, its series resistance remains connected to ground.

This form is finite at DC and preserves conjugate symmetry in frequency. It also shows that the capacitor modifies the direct transfer function.

By superposition, each source can be analyzed with the other one deactivated (figure 7.6). The active source drives its node through R_S; that node is loaded by R_L and, through C_M, by the opposite branch, which is terminated in $R_L \parallel R_S$. H_D is the voltage at the source's own node and H_C the voltage at the node of the deactivated branch.

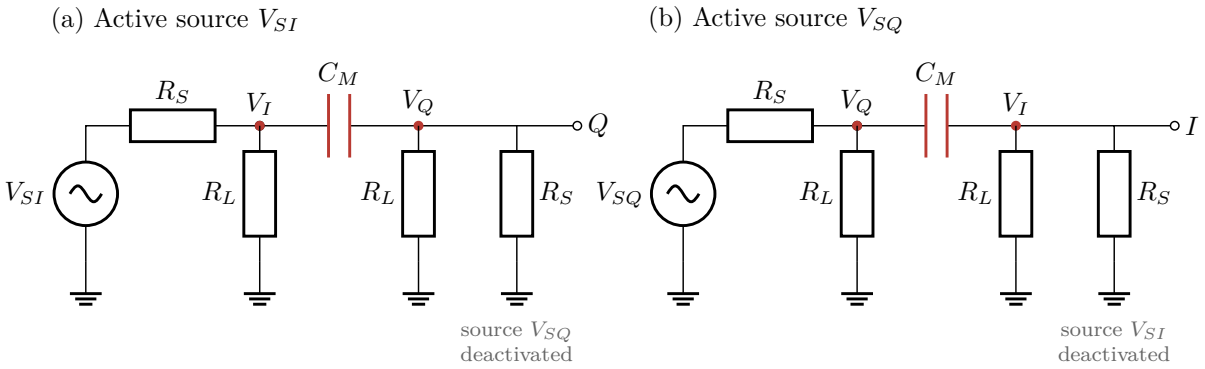

Figure 7.6: Superposition in the circuit of figure 7.5: (a) the I branch couples into the Q branch; (b) the Q branch couples into the I branch. The deactivated source leaves its series resistance connected to ground.

7.4 Magnitude, phase and modulated signal

For $R_S = R_L$, $a = 1/2$. For $x > 0$,

$$g_D = |H_D| = \frac{1}{2}\sqrt{\frac{1+x^2}{1+4x^2}}, \qquad \theta_D = \arctan x - \arctan(2x), \tag{7.9}$$

$$g_C = |H_C| = \frac{x}{2\sqrt{1+4x^2}}, \qquad \theta_C = \frac{\pi}{2} - \arctan(2x). \tag{7.10}$$

To keep A_m as the nominal amplitude without coupling, the sources must have amplitude $2A_m$ in this case. For a positive-frequency tone,

$$z(t) = De^{j\omega_m t} + Ee^{-j\omega_m t}, \tag{7.11}$$

$$D = 2A_m H_D(\omega_m), \qquad E = 2jA_m H_C^*(\omega_m). \tag{7.12}$$

The image phase is $\pi/2 - \theta_C$, not θ_C. In the weak-coupling limit, $\theta_C \to \pi/2$, while the image phase tends to zero. At DC, the cross-coupling magnitude is zero and its phase is undefined.

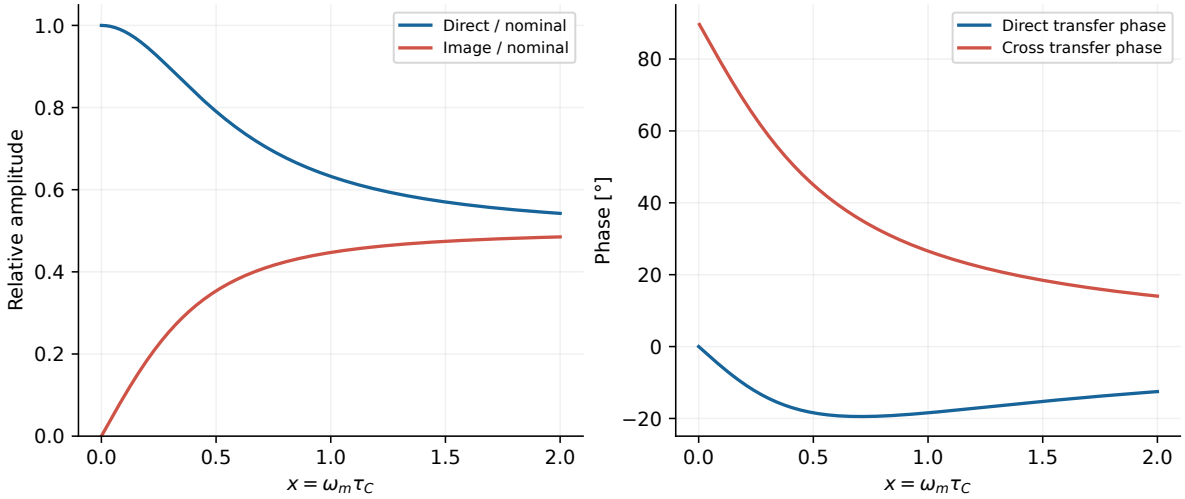

Figure 7.7: Amplitudes referred to the nominal signal, and phases of the transfer functions of the symmetric circuit. The phase of the cross transfer function is not directly the phase of the RF image.

The image ratio relative to the actual desired signal is

$$\left|\frac{E}{D}\right| = \frac{|x|}{\sqrt{1+x^2}}, \qquad L_{\text{img}} = 20\log_{10}\frac{|x|}{\sqrt{1+x^2}}. \tag{7.13}$$

Three references are distinguished: direct gain relative to A_m, image level relative to A_m, and image relative to $|D|$.

Table 7.1: Capacitive circuit: values computed with equation (7.8). D/A_m and E/A_m denote relative magnitudes.

x	g_D	g_C	D/A_m [dB]	E/A_m [dB]	Image [dBc]
0.10	0.49274	0.04903	-0.13	-20.17	-20.04
0.50	0.39528	0.17678	-2.04	-9.03	-6.99
2.00	0.27116	0.24254	-5.31	-6.28	-0.97

At $x = 0.1$, $g_C = 0.04903$ and $|E| = 0.09806A_m$. At $x = 0.5$, the image is at $-9.03\,\text{dB}$ relative to the nominal amplitude, but at $-6.99\,\text{dBc}$ relative to the actual desired signal. As $x \to \infty$,

$|D| = |E| = A_m/2$: both components lie at $-6.02\,\mathrm{dB}$ relative to the nominal amplitude and the image rejection is $0\,\mathrm{dB}$. Figure 7.8 shows the components for three degrees of coupling: with $x \simeq 0$ the image is negligible; at $x = 0.5$ the direct component is attenuated and delayed while the image grows; with $x \gg 1$ both have nearly equal magnitude and the trajectory tends toward the 45° line.

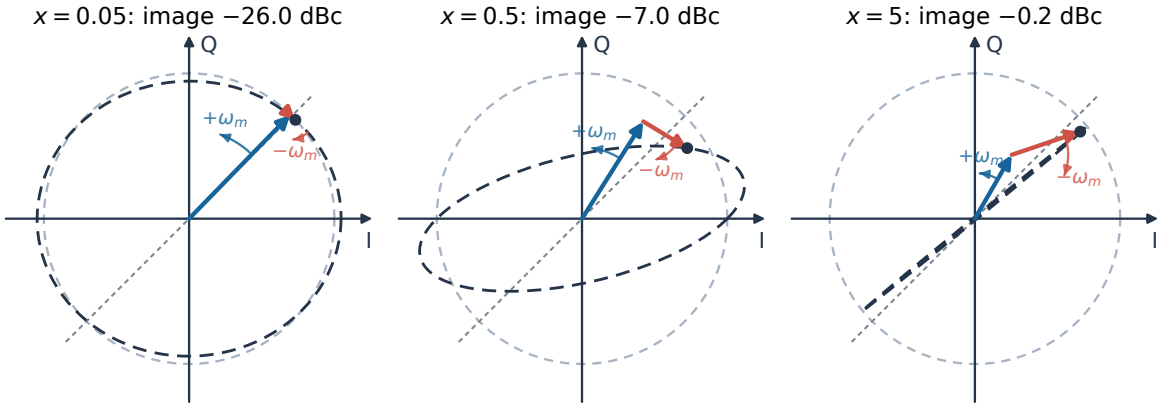

Figure 7.8: Desired (blue) and image (red) components of the symmetric capacitive circuit for $x = 0.05$, 0.5 and 5. The dotted line indicates the 45° direction.

For $x \to 0$ the circle is recovered. Increasing coupling produces attenuation and a phase shift of the direct component, together with a growing image. The equal-magnitude limit makes the inversion of the system singular: no finite predistortion can recover two degrees of freedom through a single effective direction. Since the circuit is LTI, multiple tones superpose without interacting. Figure 7.11 shows two tones of equal nominal amplitude: the image of the higher-frequency tone is larger, as expected for capacitive cross-coupling, and its direct component is attenuated more.

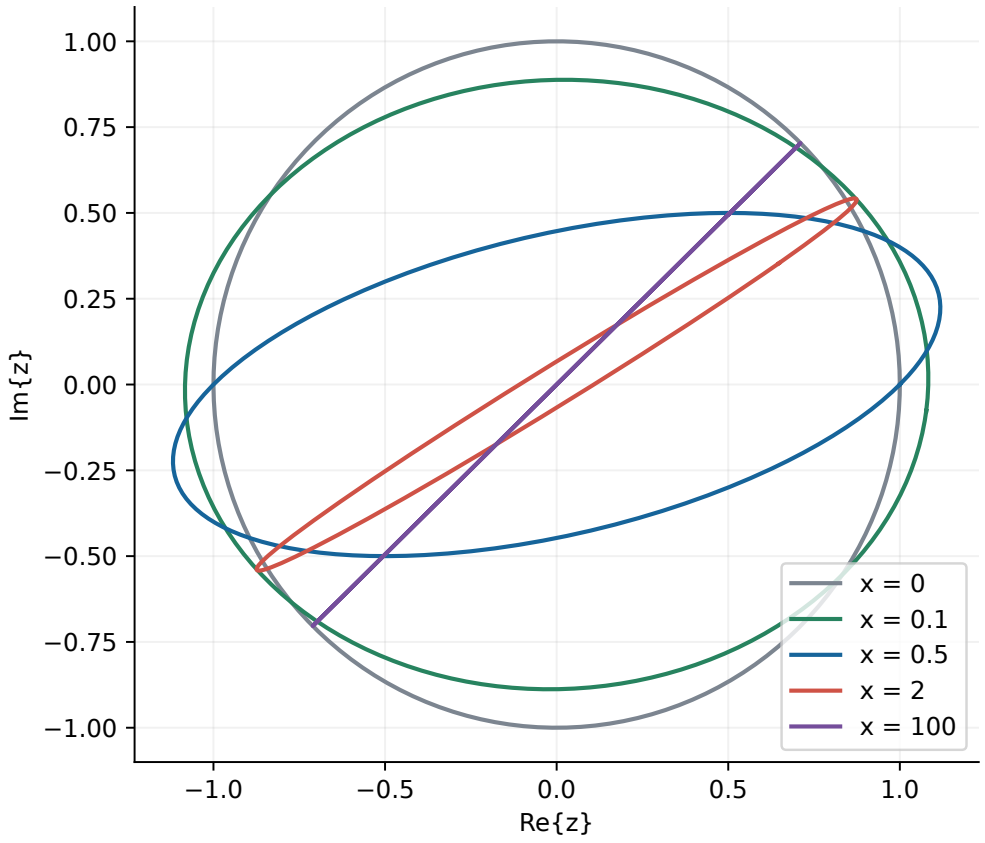

Figure 7.9: Envelope trajectories for different values of x. Strong coupling collapses the ellipse into a straight line at 45°; the desired component and the image have equal magnitude.

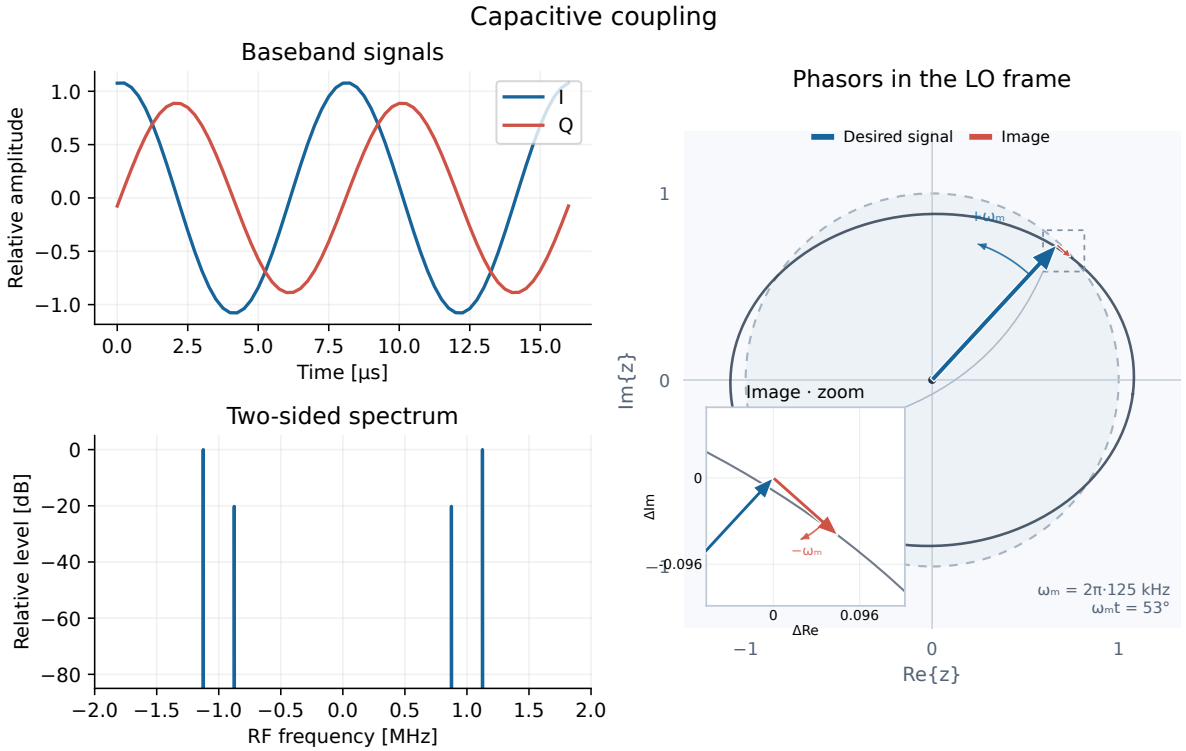

Figure 7.10: Time-domain and spectral example with $R_S = R_L = 50\,\Omega$, $C_M = 5\,\text{nF}$ and $f_m = 125\,\text{kHz}$. The sources are normalized to obtain $A_m = 1$ without coupling.

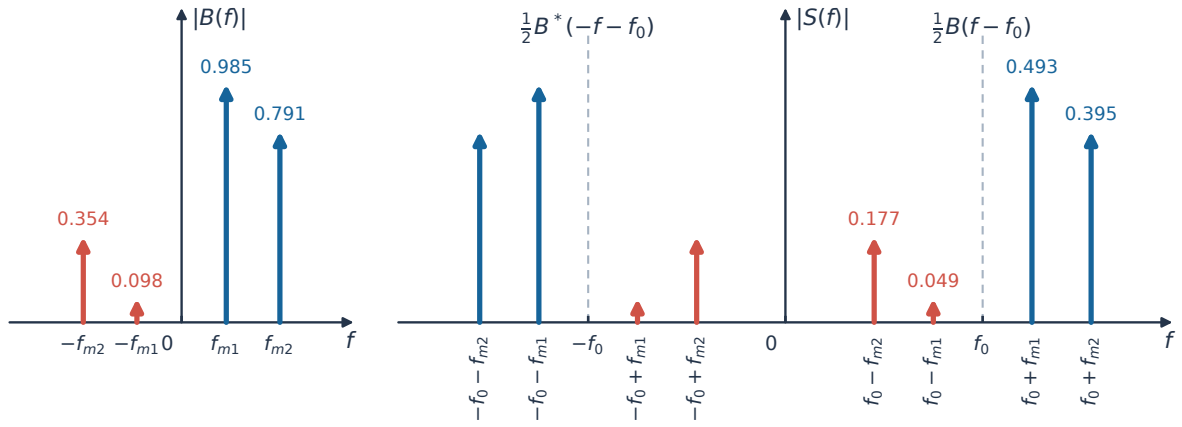

Figure 7.11: Spectrum of two tones of equal nominal amplitude in the capacitive circuit, with $x_1 = \omega_{m1}\tau_C = 0.1$ and $x_2 = \omega_{m2}\tau_C = 0.5$. The levels are computed with equation (7.8).

Chapter 8

Differential delay and combined error

8.1 Delays in the baseband branches

A time delay τ produces a phase $-\omega\tau$. In the model of figure 8.1, the delays are located in the baseband branches, before the mixers.

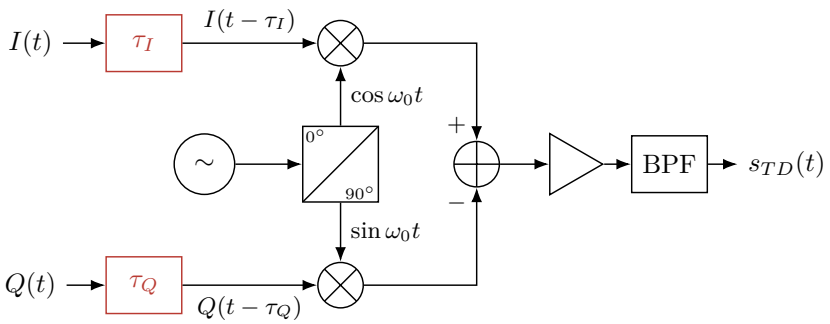

Figure 8.1: Time delays τ_I and τ_Q in the baseband branches, before the mixers.

For a tone and two constant delays,

$$b_{TD}(t) = A_m \cos[\omega_m(t-\tau_I)] + jA_m \sin[\omega_m(t-\tau_Q)]. \tag{8.1}$$

Define $\Delta\tau = \tau_I - \tau_Q$ and $\bar{\tau} = (\tau_I + \tau_Q)/2$. The decomposition is

$$b_{TD}(t) = A_m \cos(\omega_m\Delta\tau/2)e^{-j\omega_m\bar{\tau}}e^{j\omega_m t} + jA_m \sin(\omega_m\Delta\tau/2)e^{j\omega_m\bar{\tau}}e^{-j\omega_m t}. \tag{8.2}$$

Therefore,

$$D = A_m \cos(\omega_m\Delta\tau/2)e^{-j\omega_m\bar{\tau}}, \tag{8.3}$$

$$E = jA_m \sin(\omega_m\Delta\tau/2)e^{j\omega_m\bar{\tau}}. \tag{8.4}$$

For a positive sine coefficient, the image phase is $+\omega_m\bar{\tau} + \pi/2$. If one defines $\bar{\theta}_{TD} = -\omega_m\bar{\tau}$, this same phase is $-\bar{\theta}_{TD} + \pi/2$.

The RF output is always computed by taking the real part of $b_{TD}(t)e^{j\omega_0 t}$. The phase associated with the common delay depends on ω_m, because the delays in this model are located before the mixers. A delay in the complete RF chain produces a phase that depends on $\omega_0 + \omega_m$ and is a different phenomenon.

The phasor representation is analogous to that of the quadrature error, but the phase shifts added to each branch, $-\omega_m\tau_I$ and $-\omega_m\tau_Q$, grow with frequency. Since the delays do not alter the amplitudes of I and Q, the trajectory remains inscribed in the square of side $2A_m$ and flattens toward a diagonal as $f_m\Delta\tau$ increases (figure 8.3).

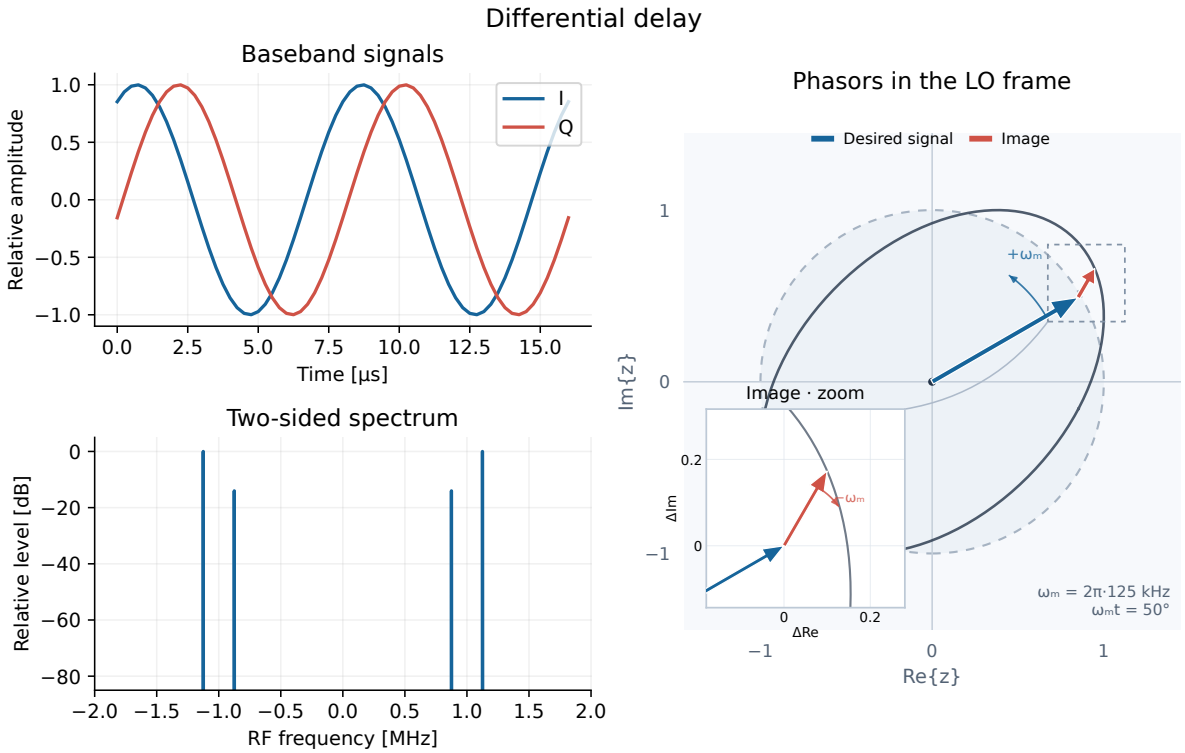

Figure 8.2: Delays $\tau_I = 0.7\,\mu$s and $\tau_Q = 0.2\,\mu$s at $f_m = 125\,$kHz. The image grows with the product of the baseband frequency and the differential delay.

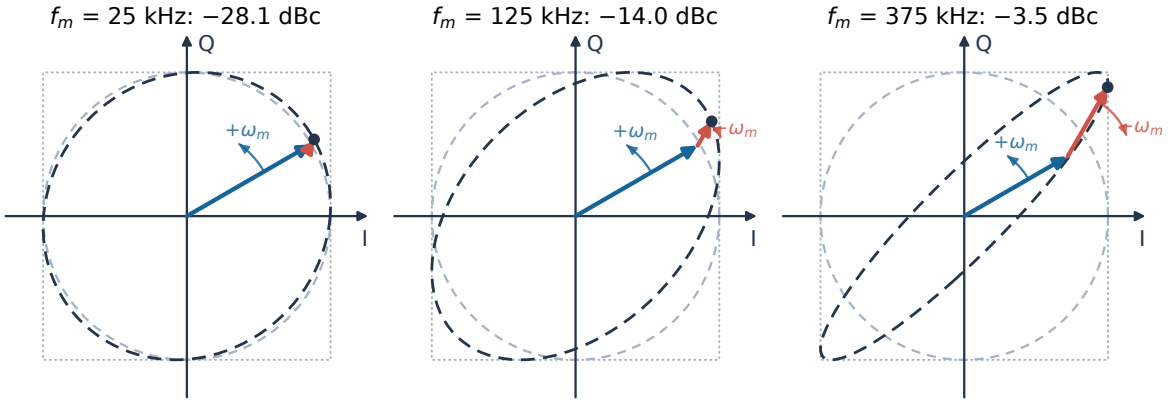

Figure 8.3: Trajectories for $\tau_I = 0.7\,\mu$s and $\tau_Q = 0.2\,\mu$s at three baseband frequencies. The dotted square marks the amplitudes of I and Q, which the delay does not modify.

8.2 Image level and narrowband approximation

$$L_{\text{img}} = 20\log_{10}|\tan(\pi f_m \Delta\tau)|. \tag{8.5}$$

The level relative to the nominal amplitude is, instead, $20\log_{10}|\sin(\pi f_m \Delta\tau)|$. The two are not interchangeable when the direct component is significantly attenuated.

In the regime $|\pi f_m \Delta\tau| \ll 1$,

$$|E/D| \simeq \pi |f_m \Delta\tau|. \tag{8.6}$$

Figure 8.4 plots both levels as a function of the product $f_m\Delta\tau$. On a logarithmic scale, the image grows at 20 dB per decade while the approximation holds. This explains the "bat wings" shape

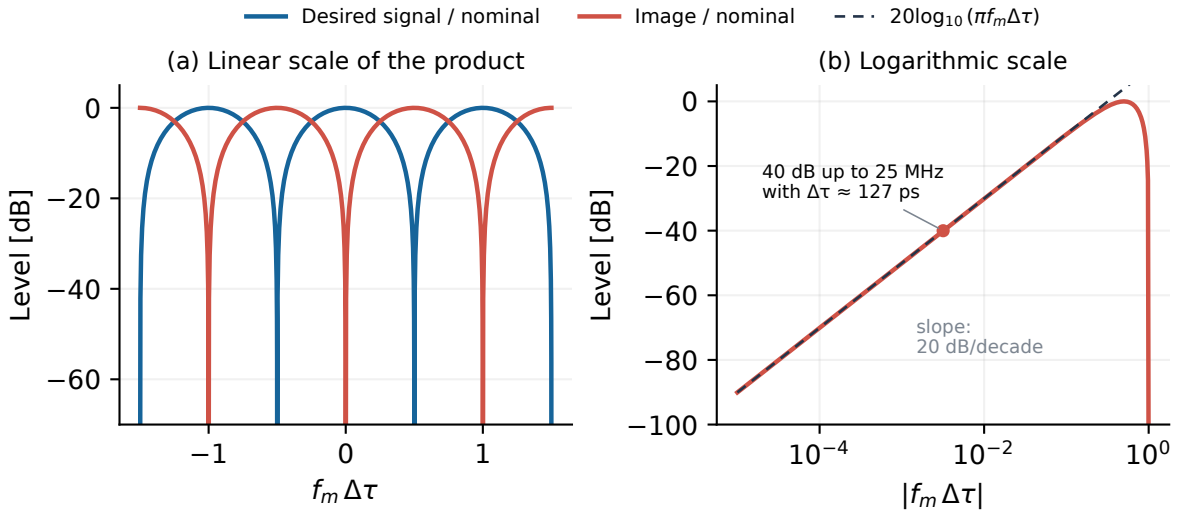

Figure 8.4: Desired signal and image, referred to the nominal amplitude, as a function of the product $f_m\Delta\tau$: (a) linear scale, with periodic zeros and maxima; (b) logarithmic scale and narrowband approximation. The dot marks the example of 40 dB up to 25 MHz.

around zero. The monotonic growth holds near that minimum, not over the entire frequency axis: the trigonometric model has other zeros and maxima. If an IRR of R_{obj} is required up to $|f_m| = F$, the approximation gives

$$|\Delta\tau| \lesssim \frac{10^{-R_{\text{obj}}/20}}{\pi F}. \tag{8.7}$$

For example, 40 dB up to 25 MHz requires approximately 127 ps if only delay imbalance is present. A gain or quadrature error consumes part of the available budget.

8.3 Simultaneous LO quadrature error and delay

Inserting the delayed channels into equation (6.1), the trigonometric products directly yield

$$\begin{aligned} s(t) = {} & A_m \cos\left(\frac{\Delta\phi - \omega_m\Delta\tau}{2}\right)\cos[(\omega_0+\omega_m)t + \bar{\phi} - \omega_m\bar{\tau}] \\ & - A_m \sin\left(\frac{\Delta\phi + \omega_m\Delta\tau}{2}\right)\sin[(\omega_0-\omega_m)t + \bar{\phi} + \omega_m\bar{\tau}]. \end{aligned} \tag{8.8}$$

Its equivalent complex coefficients are

$$D = A_m \cos\left(\frac{\Delta\phi - \omega_m \Delta\tau}{2}\right) e^{j(\bar{\phi} - \omega_m \bar{\tau})}, \tag{8.9}$$

$$E = jA_m \sin\left(\frac{\Delta\phi + \omega_m \Delta\tau}{2}\right) e^{j(\bar{\phi} + \omega_m \bar{\tau})}. \tag{8.10}$$

The difference and the sum that appear in the two terms must be preserved. It is not correct to use a single effective differential phase for both gains without deriving the model.

The image null near the origin satisfies

$$f_{m,\min} = -\frac{\Delta\phi}{2\pi\Delta\tau}, \qquad \Delta\tau \neq 0. \tag{8.11}$$

Other nulls exist when $\Delta\phi + 2\pi f_m \Delta\tau = 2k\pi$. The null of interest may fall outside the operating band. If $\Delta\tau = 0$, the quotient in equation (8.11) must not be used: the image does not exhibit that frequency dependence.

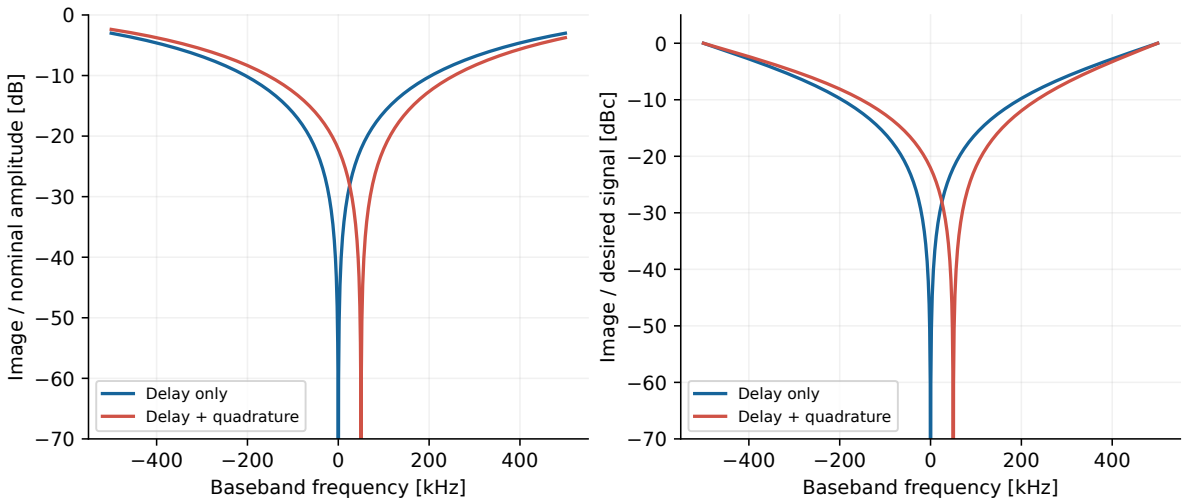

Figure 8.5: With $\Delta\tau = 0.5\,\mu$s and $\Delta\phi = -9°$, the minimum shifts to 50 kHz. The plot distinguishes the nominal reference from the actual desired signal.

Canceling the image at one frequency is not equivalent to correcting the modulator over the whole band. At that point the direct gain may differ from one, and its phase also changes. Adjusting the LO error until the minimum is shifted to zero baseband frequency removes its intercept under these assumptions, but leaves the differential delay uncorrected.

Figure 8.6 illustrates this with three baseband tones at 25, 50, and 75 kHz. With the LO error, the image of the 50 kHz tone vanishes and the other two remain at the same level, −28.1 dB. When the quadrature is corrected, the null returns to f_0 and the images grow with frequency because of the delay.

8.4 Phase delay and group delay

A real filter does not necessarily have linear phase. For a response $H(\omega)$ with unwrapped phase $\theta(\omega)$,

$$\tau_p(\omega) = -\frac{\theta(\omega)}{\omega}, \qquad \tau_g(\omega) = -\frac{d\theta(\omega)}{d\omega}. \tag{8.12}$$

For a pure delay, both quantities coincide. An all-pass filter can keep unit magnitude while modifying the group delay: the edges and the envelope of pulses change even though the magnitude

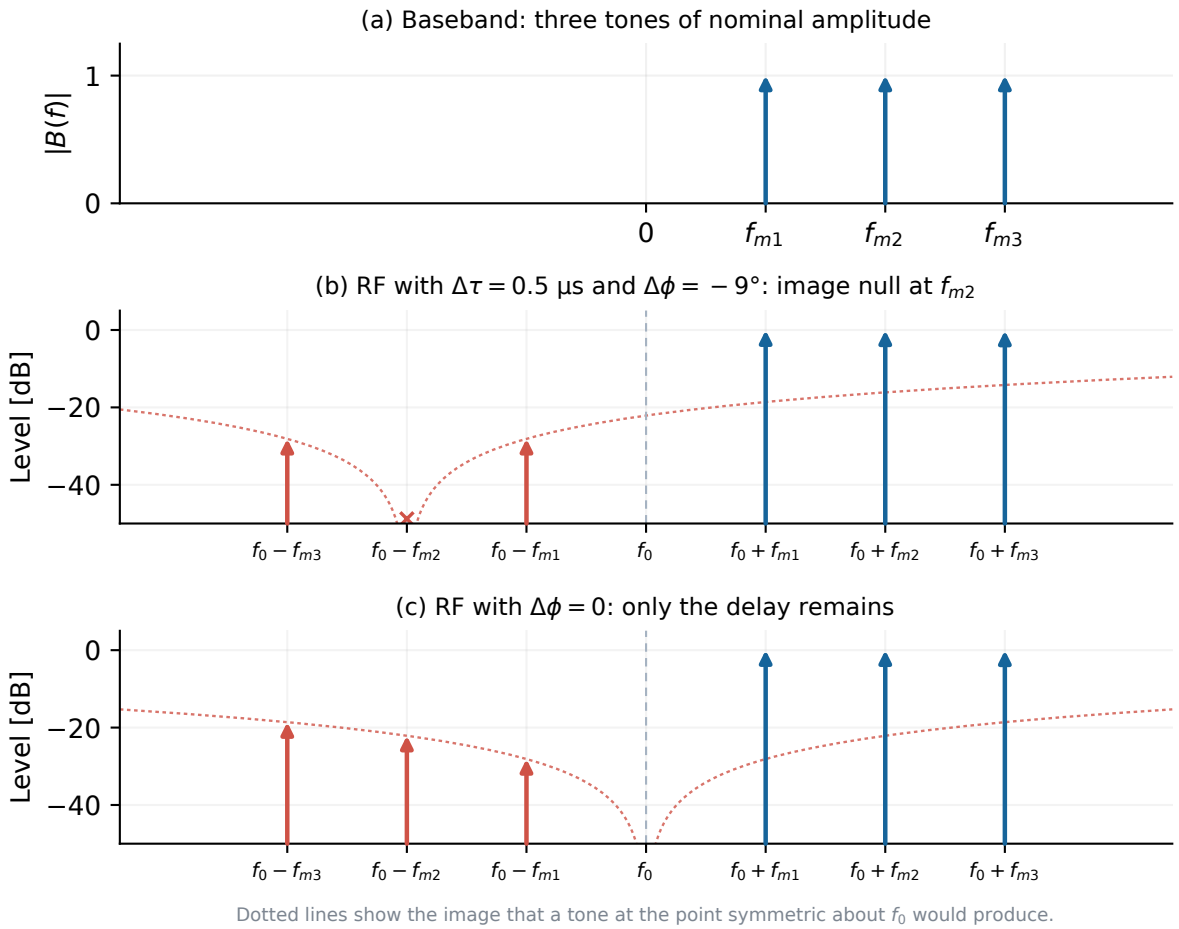

Figure 8.6: Three tones with $\Delta\tau = 0.5\,\mu$s: (a) baseband; (b) RF with $\Delta\phi = -9°$, whose image null coincides with $f_{m2} = 50\,$kHz (×); (c) RF with $\Delta\phi = 0$. Levels referred to the nominal amplitude.

at each frequency remains the same. The phase delay requires care at zero; the phase and its derivative are no longer reliable where the magnitude is zero or below the measurement floor.

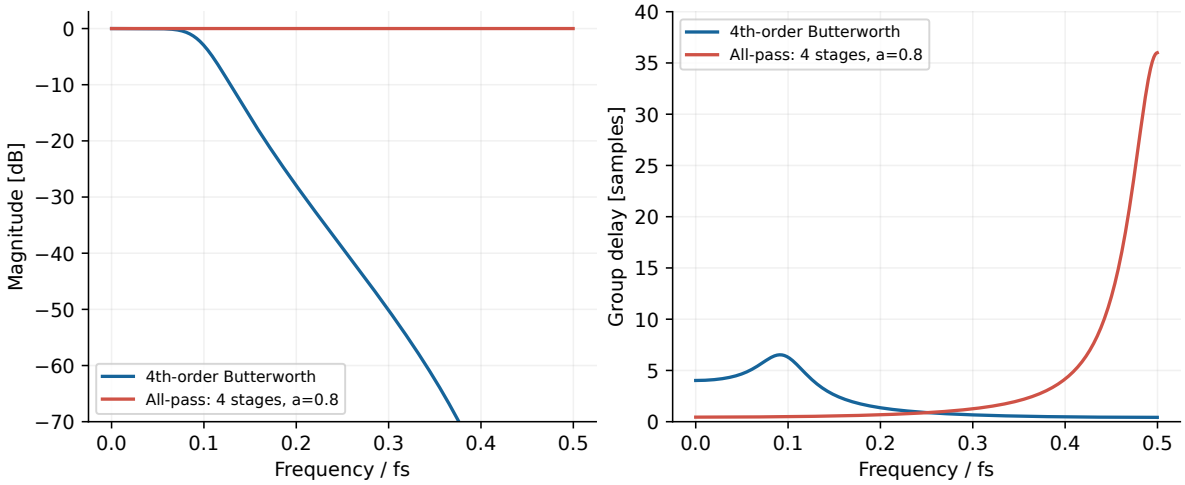

Figure 8.7: Example filters: Butterworth filter of order 4 and a four-stage all-pass cascade, with explicit coefficients.

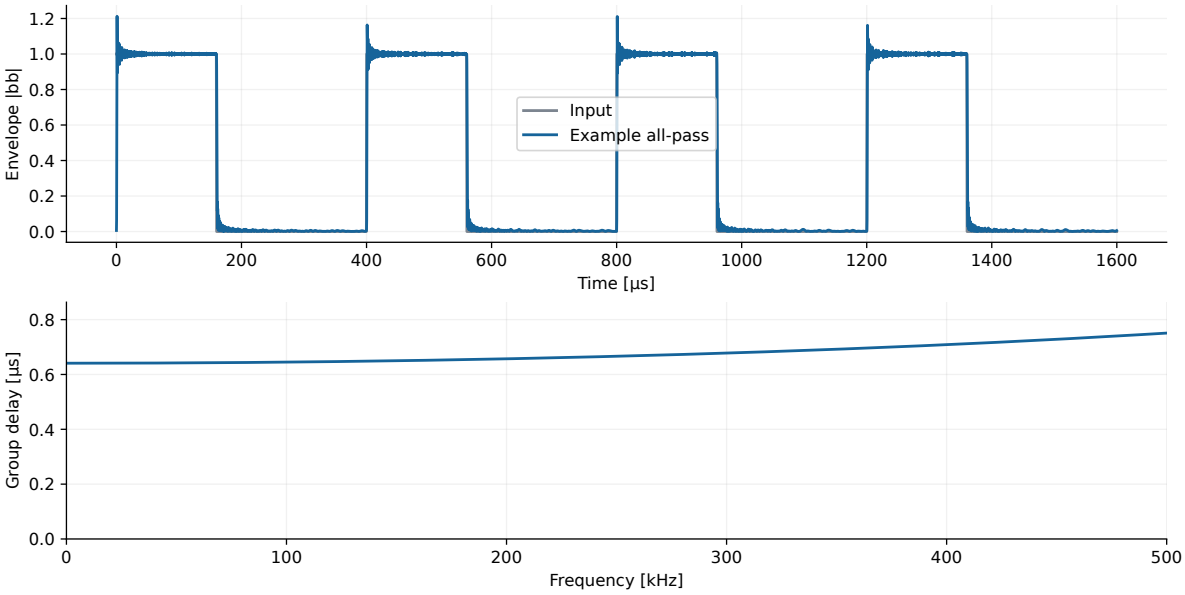

Figure 8.8: Alternating train of tones at 125 and 250 kHz, filtered with an example all-pass. The frequency-dependent delay modifies the temporal alignment of the pulses.

Chapter 9

Unified model and predistortion

9.1 Model with a conjugate term

The combination of constant linear errors can be described as

$$z(t) = \alpha b(t) + \beta b^*(t) + c. \tag{9.1}$$

α affects the direct signal, β its image, and c the leakage referred to the LO frame. This model is called widely linear because it contains both the complex variable and its conjugate. It is equivalent to an affine transformation of the two real coordinates.

The coefficients of individual errors must not be added without considering the order of the operations. Cascading two blocks, $y = \alpha_1 b + \beta_1 b^*$ and $z = \alpha_2 y + \beta_2 y^*$, yields

$$\alpha = \alpha_2\alpha_1 + \beta_2\beta_1^*, \qquad \beta = \alpha_2\beta_1 + \beta_2\alpha_1^*. \tag{9.2}$$

Offsets are also transformed as they pass through the subsequent stages. For a physical system it is preferable to build the matrix of the chain or to estimate its effective coefficients from a coherent observation.

9.2 Inversion of the constant model

To produce a desired envelope z_d, one solves

$$\begin{bmatrix} z_d - c \\ z_d^* - c^* \end{bmatrix} = \begin{bmatrix} \alpha & \beta \\ \beta^* & \alpha^* \end{bmatrix} \begin{bmatrix} b_{\text{pre}} \\ b_{\text{pre}}^* \end{bmatrix}. \tag{9.3}$$

If $\Delta = |\alpha|^2 - |\beta|^2 \neq 0$,

$$b_{\text{pre}} = \frac{\alpha^*(z_d - c) - \beta(z_d^* - c^*)}{|\alpha|^2 - |\beta|^2}. \tag{9.4}$$

The formula corrects gain, phase, cross-mixing, and offset in the constant model. Near $\Delta = 0$, the inverse greatly increases the amplitude and the sensitivity to noise or to estimation errors. In a modulator with a small image, the goal is to reduce $|\beta/\alpha|$ without consuming the output headroom; the aim is not to invert a physical degeneracy.

9.3 Frequency-dependent extension

For the LTI system of equation (7.1), the output envelope has the form

$$Z(f) = A(f)B(f) + C(f)B^*(-f), \tag{9.5}$$

$$A(f) = \frac{H_{II} + H_{QQ} + j(H_{QI} - H_{IQ})}{2}, \tag{9.6}$$

$$C(f) = \frac{H_{II} - H_{QQ} + j(H_{QI} + H_{IQ})}{2}. \tag{9.7}$$

Here $C(f)$ is the image coefficient, not the capacitance C_M. The responses on the right-hand side are evaluated at f. The mirrored frequencies are grouped together in order to invert

$$\begin{bmatrix} Z(f) \\ Z^*(-f) \end{bmatrix} = \begin{bmatrix} A(f) & C(f) \\ C^*(-f) & A^*(-f) \end{bmatrix} \begin{bmatrix} B(f) \\ B^*(-f) \end{bmatrix}. \tag{9.8}$$

The determinant is $A(f)A^*(-f) - C(f)C^*(-f)$. It cannot automatically be replaced by $|A(f)|^2 - |C(f)|^2$ without verifying the additional symmetries of the model.

A numerical inverse must be restricted to the characterized band and preserve the symmetries of the real channels. Regularization and latency can be added in order to realize stable causal filters. FFT-based filtering represents circular convolution; isolated pulses require zero padding and appropriate trimming, or an equivalent linear implementation.

9.4 Practical order of the corrections

It is useful to distinguish a common correction, which compensates the spectrum of the DAC and the filters, from a differential one, which reduces the image. The digital sequence can combine them into a filter matrix. The cancellation offset corresponding to the physical point where it is injected is then added. The final adjustment must be checked at RF, because the signal passes through all the analog blocks after the digital computation.

For a tone, a fixed phase factor can correct a delay at that frequency. For a chirp or a wideband signal, a delay requires a phase response proportional to frequency, for example a fractional-delay filter. A scalar calibration at a single tone does not demonstrate that the complete band is compensated.

Chapter 10

Calibration and verification procedure

10.1 Measurement preparation

The LO frequency, sampling rate, load, output level, and operating temperature must be fixed. The test tone must allow the desired signal, the LO, and the image to be separated. The spectral resolution and dynamic range must be sufficient to measure the target rejection. If an observation receiver is present, its own IQ imbalance must be characterized so that it is not attributed to the transmitter.

For a baseband tone $f_m \neq 0$, the following are observed:

$$f_{\text{des}} = f_0 + f_m, \quad f_{\text{img}} = f_0 - f_m, \quad f_{\text{LO}} = f_0. \tag{10.1}$$

Offsets, gain, and quadrature error can produce spectral components that are separable with this excitation [4]. A measurement of image power alone neither identifies its phase nor allows the error to be uniquely assigned to gain, LO, cross-coupling, or delay. Sweeps, additional excitation, or a coherent receiver are required to estimate the model.

10.2 Proposed sequence

1. Verify that I and Q do not saturate and that the RF operates in the linear regime. Measure the uncorrected state as a reference.
2. Minimize the LO leakage by alternating between the two DC adjustments, as in chapter 4.
3. With one tone, adjust the differential gain and quadrature to reduce the image. Alternate between both parameters and check the desired-signal amplitude.
4. Repeat with positive and negative tones distributed across the band of interest. Include points close to zero without making the lines coincide.
5. If the image changes systematically with frequency, adjust a differential delay or estimate the LTI matrix. Verify the conditioning and the headroom of the predistortion before applying it.
6. Check the LO leakage, image, gain, and phase again after combining all the corrections.
7. Validate with a representative signal, such as a chirp or a multitone, in addition to the tone used during the adjustment.
8. Repeat under the required operating conditions and record the coefficients together with the measurement parameters.

Image cancellation exactly at $f_m = 0$ cannot be measured as two separate components: signal and image coincide at the LO, and carrier leakage may also be present. To estimate the intercept of the phase error, tones close to zero are used or a model is fitted to a sweep.

10.3 FFT, coherence, and normalization

For samples $x[n]$, the FFT normalized by N approximates the amplitudes of coherent tones. A cosine of amplitude A produces two coefficients of magnitude $A/2$. The correct axis is the one defined by $\mathrm{fftfreq}(N, 1/f_s)$, and it is ordered with fftshift. An axis built from a linear interval that includes both endpoints does not exactly represent the FFT bins.

With a window $w[n]$, the normalization for the amplitude of coherent tones is by $\sum_n w[n]$, not by the size of a zero-padded FFT. Zero padding interpolates the spectrum but does not improve the physical resolution of an observation of fixed duration. An off-bin tone retains peak-reading errors and spectral leakage; the energy of a pulse or of a band is computed with the corresponding power normalization.

The simulations in this report use $N = 16384$, $f_s = 4\,\mathrm{MHz}$, and $f_m = 125\,\mathrm{kHz}$ in the tone cases. The signal, image, and LO frequencies are coherent with the observation window. The finite chirp is not interpreted as a line: its spectrum is expressed relative to an explicit nominal amplitude.

10.4 Acceptance criteria and limits

Each application must specify at least the maximum image and leakage level, the gain tolerance, the allowable phase or delay variation, and the headroom before saturation. This report does not assign acceptance thresholds to equipment that has not been specified. The evaluation must cover the band and the operating conditions, not only the best minimum of an isolated sweep.

The simulations verify algebraic identities and circuit cases. They do not model a real noise floor or environmental drift. A zero-image result in the model represents a mathematical zero, not an infinite experimental rejection.

Chapter 11

Conclusions

The complex envelope offers a compact representation of the IQ modulator, provided that the sign convention and the normalization between baseband and RF are maintained. Quadrature belongs to the axes and carriers; the I and Q channels are sine and cosine only for particular excitations.

Offsets generate a component at the LO. Gain imbalance, loss of quadrature, and differential delay introduce a conjugate term that mirrors the desired spectrum. Each mechanism can also modify the desired amplitude and phase, so minimizing the image is a necessary but not sufficient condition for preserving the signal.

Coupling between branches must be represented with a circuit or a transfer matrix. The symmetric capacitive circuit studied here allows both the cross-coupling and the direct modification to be derived. If the branches are not symmetric, the cross-coupling can also alter the direct component; a conclusion based only on a pure image is no longer valid.

Compensation can be formulated as the inversion of a model with a conjugate term, or of a filter matrix when the errors change with frequency. Its usefulness depends on the conditioning, the range of the DACs, and the quality of the estimate. A local cancellation by phase and delay does not demonstrate a wideband correction.

The report separates nominal levels from ratios in dBc, states the conditions of the models, and computes its figures and examples from them. The next experimental step is to identify the effective matrix of a specific modulator, compare its parameters against measurements, and validate the correction under the intended frequency, level, and temperature conditions.

Bibliography

[1] Richard Lyons. *Quadrature Signals: Complex, But Not Complicated*. DSP Training, November 2000.

[2] John Hansen, Agilent Technologies. *Vector Modulation and Frequency Conversion Fundamentals*, 2013.

[3] Xiaogeng Xu and Kai Wen. *Modeling and Compensation of a Non-Ideal I/Q-Modulator*. Master's thesis, Chalmers University of Technology, report EX083/2007, 2007.

[4] Eamon Nash, Analog Devices. *AN-1039: Correcting Imperfections in IQ Modulators to Improve RF Signal Fidelity*. Application note, 2009.

[5] Maxim Integrated. *Equalizing Techniques Flatten DAC Frequency Response*. Application note 3853, 2012.

[6] Massachusetts Institute of Technology, OpenCourseWare. *8.02 Physics II: Electricity and Magnetism, Summary of Class 21*. Spring 2007. Material on mutual inductance and transformers.